



TurbEFA: an interdisciplinary effort to investigate the turbulent flow across a forest clearing

RONALD QUECK^{1*}, CHRISTIAN BERNHOFER¹, ANNE BIENERT², THOMAS EIPPER³, VALERI GOLDBERG¹, STEFAN HARMANSA¹, VEIT HILDEBRAND³, HANS-GERD MAAS², FABIAN SCHLEGEL⁴ and JÖRG STILLER⁴

¹Institute of Hydrology and Meteorology, Technische Universität Dresden, Germany

²Institute of Photogrammetry and Remote Sensing, Technische Universität Dresden, Germany

³Institute of Aerospace Engineering, Technische Universität Dresden, Germany

⁴Institute of Fluid Mechanics, Technische Universität Dresden, Germany

(Manuscript received December 16, 2013; in revised form July 1, 2014; accepted July 25, 2014)

Abstract

It is assumed that the description of the exchange processes between heterogeneous natural surfaces and the atmosphere within turbulence closure models is mainly limited by a realistic three-dimensional (3D) representation of the vegetation architecture. Within this contribution we present a method to record the 3D vegetation structure and to use this information to derive model parameters that are suitable for numerical flow models. A mixed conifer forest stand around a clearing was scanned and represented by a dense 3D point cloud applying a terrestrial laser scanner. Thus, the plant area density (*PAD*) with a resolution of one cubic meter was provided for analysis and for numerical simulations. Multi-level high-frequency wind velocity measurements were recorded simultaneously by 27 ultrasonic anemometers on 4 towers for a period of one year. The relationship between wind speed, Reynolds stress and *PAD* was investigated and a parametrization of the drag coefficient C_D by the *PAD* is suggested. The derived 3D vegetation model and a simpler model (based on classical forest assessments of the site) were applied in a boundary layer model (BLM) and in large-eddy simulations (LES). The spatial development of the turbulent flow over the clearing is further demonstrated by the results of a wind tunnel experiment. The project showed, that the simulation results were improved significantly by the usage of realistic vegetation models. 3D simulations are necessary to depict the influence of heterogeneous canopies on the turbulent flow. Whereas we found limits for the mapping of the vegetation structure within the wind tunnel, there is a considerable potential for numerical simulations. The field measurements and the LES gave new insight into the turbulent flow in the vicinity and across the clearing. The results show that the zones of intensive turbulence development can not be restricted to the locations found in previous studies with more idealized canopies.

Keywords: Boundary layer model, drag coefficient; large eddy simulation, vegetation parametrization, wind field measurements, terrestrial laser scanning, wind tunnel

1 Introduction

General Problem and Motivation: A detailed knowledge of the turbulent wind field above and within forest stands is in demand among different subject areas, e.g., the assessing of storm damage risks, the modeling of the interaction between atmosphere and earth surface on larger scales and the assessment of carbon sequestration of forests and their capacity for absorption and emission of atmospheric trace gases.

Forests act as a sink, a source and a storage for atmospheric gases and energy. Horizontal exchanges of energy and mass (advective fluxes) occur as a result of the heterogeneity of the soil conditions and the vegetation composition, but sub-canopy currents of air show spatial heterogeneity especially in nonuniform tall stands and can not be measured by the commonly used

eddy covariance method (AUBINET, 2008; FEIGENWINTER et al., 2008; DUPONT et al., 2011). The flow over typical forests with clearings, paths and changing terrain level can be seen in a permanent transition, adapting to the changing surface conditions. Flux measurements suffer a positioning problem, as there exists almost no equilibrium layer and the assumption of frozen turbulence according to TAYLOR (1938) is not justified close to the canopy (for more information see AUBINET et al., 2012). Furthermore, coherent structures interfere systematically with the vertical exchange of energy and mass (FINNIGAN, 2000). All these features cause remarkable uncertainties in the assessment of the energy and mass fluxes between forests and the atmosphere.

Other Experiments: Intensive experiments to assess complete mass balances of several forest stands have revealed that measurements at discrete points unsatisfactorily represent the heterogeneity of energy and mass exchanges (AUBINET et al., 2010), and complementary flow modeling is needed. However, applications of numerical flow models to tall plant canopies are limited,

*Corresponding author: Ronald Queck, Institute of Hydrology and Meteorology, Technische Universität Dresden, 01062 Dresden, Germany, e-mail: ronald.queck@tu-dresden.de

amongst other factors, by the lack of realistic and detailed information on vegetation structure (CESCATI and MARCOLLA, 2004). The disturbance of the eddies by the local vegetation elements rules out the application of models relying on the mixing length theory. However, several studies with Reynolds-Averaged-Navier-Stokes (RANS) models showed surprising good results (ZENG and TAKAHASHI, 2000; PINARD and WILSON, 2001; SOGACHEV et al., 2002; SUN, 2005; HEINEMANN and KERSCHGENS, 2006; SOGACHEV and PANFEROV, 2006; HIRAOKA and OHASHI, 2008; SANTIAGO et al., 2010). An appropriate parametrization of the vegetation seems to be more important for realistic results than the type of turbulence closure. The influence of the canopy structure on the results of numerical flow simulations is rarely investigated, also for models which simulate the turbulent motions at least partly like large-eddy simulations (e.g. YANG et al., 2006; DUPONT et al., 2011).

Objectives: To address this topic and to improve the parametrization of unresolved exchange effects in numerical models the *TurbEFA* project was established. *TurbEFA* is the acronym for the interdisciplinary project *Turbulent Exchange processes between Forested areas and the Atmosphere*, which encompasses the work of five groups with responsibilities for: terrestrial laser scanning (TLS), meteorological field measurements (FM), wind tunnel measurements (WT), boundary layer modeling (BLM) and large-eddy simulation (LES). As a contribution to the assessment of the fluxes between the atmosphere and forests typical for Mid-Europe, we investigated the turbulent flow around a forest clearing in a combined effort by field experiments as well as by physical and numerical models. After a description of the site and the methods (Section 2 and 3) the following objectives are pursued within this article: Section 4) the improvement of methods to parametrize a tall vegetation in numerical models, Section 5) the assessment of the model sensitivity on parametrization, turbulence closure and sub-grid model and Section 6) the analysis of turbulent flow around a forest clearing and comparison of the model results and measurements.

2 Site

Subject of investigation is the *Fluxnet* site *Anchor Station Tharandt* (BALDOCCHI et al., 2001, www.fluxdata.org), which is located about 15 km southwest of the city of Dresden in Germany (latitude: 50° 57' 49" N, longitude: 13° 34' 01" E). The site has been operated by the Chair of Meteorology at the Technische Universität Dresden since 1958. In 1995, the flux measurements started on the *Fluxnet* tower (height 42 m), since then an extensive suite of meteorological, hydrological, ecological measurements and remote sensing observations have been used to investigate the climate and the exchange processes in and above the forests (FRÜHAUF et al., 1999; FEIGENWINTER et al., 2004; GRÜNWALD and BERNHOFER, 2007; MODEROW et al., 2007; SCHWÄRZEL et al., 2009; QUECK et al., 2012).

The site is embedded within the east part of a large forested area called the *Tharandter Wald* (7120 ha), which is a tableland with few hillocks and narrow valleys at the border. The presented experiment focuses on the forest clearing *Wildacker* (approximate size 50 m × 90 m) in the vicinity of the site around 130 m west of *Fluxnet* tower. A small hillock, the *S-Berg*, is located five hundred meter further west (see Fig. 1 and 2), giving the site an average terrain inclination of about 6 %.

The Norway Spruce (*P. abies*) stand around the *Fluxnet* tower was seeded in 1887, but is composed of 87 % coniferous evergreen and 13 % deciduous. The stand is characterized by the dense canopy of the mature spruce stand (approximate height $h = 30$ m) and an open trunk space with sparse understory. Grasses cover approximately 50 % of the ground within the stand. The *Wildacker* is surrounded by a belt of chestnuts (*Castanea*) which smooths the forest edge and closes the trunk space.

3 Methods

3.1 Terminology

Frequently used variables

PAD	single-sided plant area per unit volume	in	m^2/m^3
PAI	single-sided plant area per ground area	in	m^2/m^2
C_D	drag coefficient		
h	canopy height	in	m
u, v, w	wind components: stream-wise, lateral and vertical	in	m/s
z	height above ground	in	m

An overbar denotes a time average and a prime fluctuations about time average. Angle brackets represent spatial means. The reference position is the top of *Fluxnet* tower (42 m, tower T4, see Fig. 3). The field measurements, the wind tunnel measurements as well as the results of the numerical simulations are normalized with results from the respective position. Further we define the acronyms:

TLS	terrestrial laser scanning
FM	meteorological field measurements
WT	wind tunnel
BLM	boundary layer modeling
LES	large-eddy simulation

3.2 Vegetation assessment

3.2.1 Survey

Following the concept of Rayleigh the drag force experienced by vegetation due to atmospheric motion is usually calculated from the PAD or the single-sided plant area index (PAI , i.e. the PAD integrated over the stand height). Beside the method of harvesting the plants and



Figure 1: Topography of the *Tharandter Wald* in the vicinity of the site. The location of the *Fluxnet* tower T4 is marked by the target, using Gauß-Krüger coordinates T4 is located at Easting 5399344 m, Northing 5648455 m. The dotted area in the west of the tower indicates the clearing *Wildacker*.

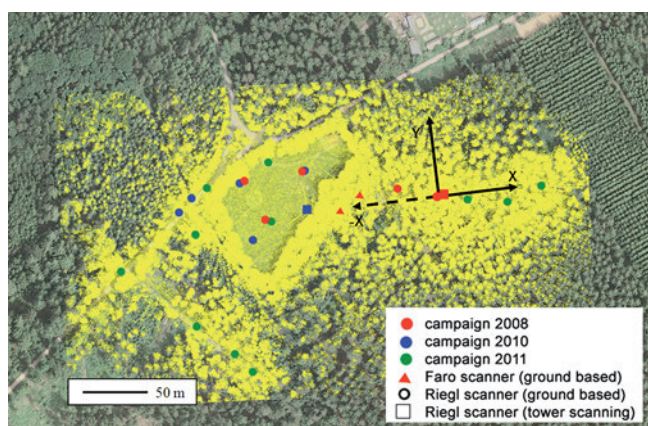


Figure 2: Digital orthophoto of the field site (ATKIS®-DOP® Staatsbetrieb Geobasisinformation und Vermessung Sachsen 2013) overlaid with the terrestrial laser scan data recorded between 2008 and 2011, point cloud was thinned for printing purpose.

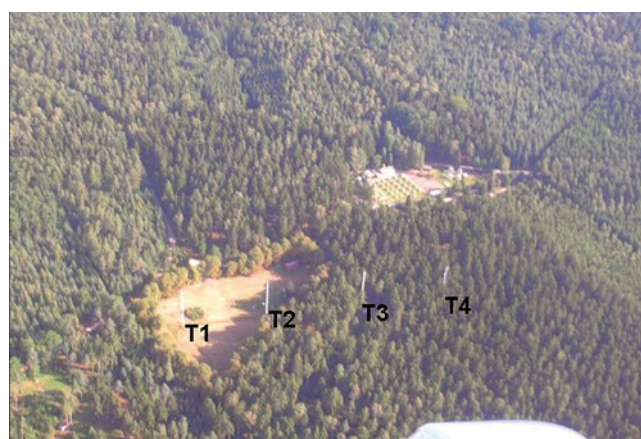


Figure 3: Aerial photo of the site (courtesy of W. JUNKERMANN, 31.07.2008), the four measurement towers build a transect over the clearing from West (T1) to East (T4 the *Fluxnet* tower), almost parallel of latitude.

measuring the *PAI* directly, there exists several indirect methods like forest assessments (using allometric functions) or optical measurements (measuring the gap fraction of the canopy).

Here, the *PAI* is determined on the basis of a forest assessment from 1999 (including the harvest and analysis of 6 Norway spruces). Using this assessment, continuous in-canopy radiation measurements (since 1996) as well as measurements with a plant canopy analyzer PCA LAI-2000 (LiCOR, Lincoln, NE), the *PAI* was estimated to be $7.1 \text{ m}^2/\text{m}^2$ in 2008.

Recent developments allow the application of laser scanning to forest stands. Based on TLS we developed a method to derive a detailed 3D representation of the forest stand suitable for numerical modeling. Laser scan-

ning is a precise 3D measurement technique, which can be used as a fast and efficient tool to obtain dense 3D point clouds representing the vegetation structure (VOSSELMAN and MAAS, 2010). The size of the covered area depends on the scanner platform: Airborne laser scanners may be employed to cover wide areas, while terrestrial laser scanning conducted on static tripods delivers very high 3D point densities for a limited area. Both may be used simultaneously for *PAD* related data acquisition whilst the point clouds complement each other.

3.2.2 Terrestrial and airborne laser scanning data

From summer 2008 till autumn 2011, several laser scanning campaigns were conducted on windless days to

record the vegetation under leaf-off and leaf-on conditions. The site was primarily scanned with a terrestrial laser scanner Riegl LMS-Z 420i (Riegl Laser Measurement Systems, Austria); on two positions a Faro LSHE80 (Faro Europe GmbH&Co. KG, Germany) laser scanner was used. Further details to the scanner specification are given in RIEGL (2009) and FARO (2005).

In total, the study site was recorded from 25 different laser scanner positions, conducted in three different measuring campaigns. Two positions at the top of two towers (*Fluxnet* tower (T4) inside the Norway Spruce stand and a scaffolding tower (T2) on the clearing), which are approximately 10 m above canopy, were chosen to provide a high resolution canopy coverage. The distribution of the scan positions is shown in Fig. 2. The scans are merged into a single 3D representation of the object by using an automatic software tool matching tie points (retro-reflective cylinders and white spheres) (BIENERT and MAAS, 2009). We apply a right-handed coordinate system, where the X-axis points eastwards along the transect of the towers and the Y-axis points northwards.

As a basis for calculations for a larger area we deployed the digital terrain model (DTM, ATKIS®-DGM2¹). It is based on airborne laser scanner (ALS) data and has a grid spacing of 2 m and an average height accuracy of the grid points of 20 cm.

Raw airborne laser scanner data (first and last echo), recorded in spring 2006, were utilized to derive the canopy surface model using a simple maximum filtering method with a grid spacing of 2 m. Then the ALS canopy height model was obtained by subtracting the DTM from the canopy surface model.

3.2.3 Co-registration of airborne and terrestrial laser scan data

A combined analysis of airborne laser scanner data (which are geo-referenced) and terrestrial laser scanner data (in a local coordinate system) requires a co-registration. A method was used, which matches tree positions extracted from both data sets. A detailed description is given in BIENERT et al. (2011). The major part of the trees are coniferous species, which are well suited for reliable automatic tree top detection. The tree tops were extracted from the ALS data, representing the tree position at canopy level. In the TLS data, the tree position was extracted by detecting the stem center at breast height (MAAS et al., 2008). To get an uniform height base, the positions are reduced to the current DTM heights. Finally, a matching of the tree position was performed, applying the RANSAC algorithm (FISCHLER and BOLLES, 1981) to determine the transformation parameters, automatically removing spurious detections.

¹The digital terrain model (ATKIS®-DGM2) and the raw ALS data were obtained from the GeoSN (Staatsbetrieb Geobasisinformation und Vermessung Sachsen).

3.2.4 Voxel based representation of the vegetation structure

As a basis for an application in numerical simulations and an efficient handling of the unorganized point clouds with a huge number of data points, a regular grid structure (voxel space) was chosen. A voxel V_i is a cube on a discrete position in a Cartesian coordinate system. Thus, a structure of equidistant and orthogonal voxels represents a voxel space.

The approach, which was presented in BIENERT et al. (2010) and QUECK et al. (2012), uses the scanner position together with the pulse direction to ascertain whether the pulse passed through a voxel or not. As the probability that a beam is intercepted in a voxel, P_{total} of each voxel V_i represents the projected PAD.

Optical measurements suffer from the occlusion of the beams penetrating the canopy. Therefore so called clumping factors are used to scale the optical measurements on the direct assessments (i.e. harvesting methods). Compared to measurements of common gap light analyzers, the presented approach uses different view points around an object which should reduce the probability of occlusion significantly. However, for the area around tower T4 we received only a value of $\int_0^h \langle P_{\text{total},T4} \rangle = 2.0$, which is similar to the values obtained with the PCA LAI-2000. Compared to the LAI = 7.12 from forest assessments and to estimates from literature this is very low. Therefore we scaled the P_{total} by a factor of 3.6 to match the plant area index obtained from forest assessments. For further details about the presented method please refer to BIENERT et al. (2010) and QUECK et al. (2012).

3.2.5 Virtual canopy generator

The computational domain for numerical simulations should be large enough to allow for the development of the relevant turbulence structures (e.g. coherent structures). A solution to extend the scanned voxel space was delivered by BOHRER et al. (2007), who presented a ‘virtual canopy generator’ for building a heterogeneous forest based on statistical data. The generated canopy preserves the mean biological features of the forest stand, but differs from reality when looking at the explicit fine details.

For the application of the virtual canopy generator the forested area covered by the computational domain is decomposed into a number of forest plots. For each of them various statistical information are available from local observations, e.g., mean tree height, diameter at breast height or a mean PAI. Furthermore, a so called random canopy field has to be provided plot-wise that prescribes the horizontal structure of the contained vegetation. The ALS canopy height model, described in Section 3.2.2, contains the local tree height h with the desired resolution for each forest plot and, hence, it is used as random canopy field. With this information, the virtual canopy generator creates a local PAI on an equidistant, orthogonal (voxel) mesh of 2 m resolution for the

whole computational domain. Generic profiles of [PETERS and EIDEN \(1992\)](#) and [KRAUS \(2008\)](#) are applied to calculate the *PAD* based on the generated *PAI* and the known tree height h . Finally, the virtual forest is replaced by the measured one where terrestrial laser scanning data are available. For more details on the virtual canopy generator we refer to [BOHRER et al. \(2007\)](#) and for its application to the current forest to [SCHLEGEL et al. \(2014\)](#).

3.3 In situ wind measurements

3.3.1 Experimental design

The main experiment within the *TurbEFA* frame took place from May 2008 to May 2009. In a preceding experiment, carried out from June 2007 to November 2007 and called *WinCanop*, high resolution wind profiles within and above the canopy were recorded at the *Fluxnet* tower. Based on these results the design of the spatially more extended *TurbEFA* experiment was optimized.

The investigated domain is aligned west to east according to the predominant wind direction and includes the clearing *Wildacker*. In the aerial photo in Fig. 3 one can detect four measurement towers. On the far right side, 100 m east of the clearing, the *Fluxnet* tower (T4) is located in an almost homogeneous forest stand. During the *TurbEFA* experiment three additional towers were erected: the telescoping tower T1 near the leading edge of the clearing and two scaffolding towers T2 and T3 right in front and approximately 40 m behind the eastward forest edge. The origin of the local coordinate system was defined at the base of the *Fluxnet* tower (T4).

3.3.2 Wind measurements

Table 1 gives the location of the towers T1, T2 and T3 relative to T4 as well as the mounting positions of the ultrasonic anemometers (Sonics). Additionally, measurements on 2 m pillars were conducted at five positions along the transect in between of the towers (see Fig. 19). From these 31 measurement positions, a frame of 19 positions was operated permanently at the four towers (heights: 2 m, 10 m, 20 m, 30 m, 40 m), the remaining 12 positions were operated temporarily by moving instruments.

3.3.3 Data processing

The Sonic signals were sampled with 20 Hz simultaneously and all raw data were stored. In post-processing the raw data of the wind vector were rotated in a single coordinate system and combined to half hourly statistics.

Several quality tests (see [AUBINET et al. 2012](#)) were included in the routines. We applied limits for wind components (± 30 m/s) and Sonic temperature (25 °C to 40 °C) on the 20 Hz data. Further, the difference between

Table 1: Sensor positions at the towers in m.

Horizontal positions (respective to Gauß-Krüger coordinates: Easting 5399000, Northing 5648000)				
Position name	T1	T2	T3	T4
Easting	179	231	292	344
Northing	439	440	446	446
Height ASL	388	386	386	385
Distance to T4	165	113	52	0
Level name	Sensor heights			
5		40.0	40.0	42.0
				33.0
4	31.0	30.0	30.0	30.0
			24.0	25.0
3	20.6	20.0	20.0	20.0
	16.0	15.0		
2	11.5	10.0	10.0	10.0
	5.3	5.0		
1	2.0	2.0	2.0	2.0

consecutive data points was used to detect spikes, the method proposed in [CLEMENT \(2004\)](#) regards dropouts too. Stationarity tests were applied after [FOKEN and WICHURA \(1996\)](#), and times with precipitation were excluded to avoid artifacts.

In general, winds from west (wind sector: 255 ° to 285 °, based on measurements on T4 at 42 m) are investigated because this is the most frequent wind direction as well as this is in line with the model domain and the tower setup. In addition to these constraints, we restricted the investigated data set to near neutral thermal stratification by a range of the stability index (z/L) from -0.1 to 0.1 (where L is the Monin-Obukhov length).

3.4 Wind tunnel

3.4.1 Experimental set-up

The wind tunnel measurements took place in the boundary layer wind tunnel of the Institute of Aerospace Engineering, Technische Universität Dresden. It has a cross section of 1.4 m \times 1.4 m and an overall length of 16 m, which includes a measurement section of 8 m length.

According to the minimal domain size and the spatial resolution of the requested results a scale of 1:450 was chosen for the physical model. Thus, the effect of both, vegetation and the topography, could be considered.

The adjustable ceiling of the WT allows to set up the pressure gradient within the measurement section as small as possible. An atmospheric boundary layer according to a logarithmic wind profile has been established following the DIN 1055 ([ROSEMEIER, 2009](#)). The boundary layer was generated and adjusted by the use of three vortex generators ([ARMITT and COUNIHAN, 1968](#)) and roughness elements (steel brackets with two different heights, z_0 and $2z_0$) over a length of 5 m in front of the measurement section (see Fig. 4, left side).



Figure 4: Left side: view along the wind tunnel. The Counihan vortex generators in the background are followed by the steel brackets and rectangular arranged roughness elements over the *S-Berg*, and, finally, the site model in the foreground. Right side: a close-up of the site model.



Figure 5: An artificial forest stand build by conventional tree models (left) and cylindrical wire frames (right).

3.4.2 The configuration of the site model

The elevation of the terrain including the *S-Berg* in the west of the *Wildacker* was modeled by styrofoam.

The aerodynamic properties (e.g. permeability) of small tree models, which are commonly used in wind tunnels (e.g. FRANK and RUCK, 2008), are different from real trees, in spite of the apparent similarity.

AUBRUN *et al.* (2005) suggested cylindrical wire frames to reproduce the aerodynamic characteristics of the canopy structures. After initial tests with both model types we used wire frames with a diameter of 40 mm (i.e. 18 m in the model scale, see Fig. 5). Each of these intertwined cylinders represents a cluster of trees.

3.4.3 Measuring techniques

To capture the mean velocity profiles hot wire anemometers (HDA) were used. The finest spatial resolution of the measurements is given by the wire length of 1 mm, corresponding to a length of 0.45 m in the field. Along with a sample frequency of 1250 Hz (corresponding 2.8 Hz in situ) a sufficient spatial and temporal resolution is provided.

Having stationary flow conditions within the wind tunnel, we recorded vertical profiles by sampling intervals of 20 s at each position. The means over these intervals are comparable to an in situ mean over 15 min.

3.5 Atmospheric boundary layer model

The two-dimensional atmospheric boundary layer model (HIRVAC-2D) was designed as a tool for fast calculation of flows over surface inhomogeneities. Within HIRVAC

a standard set of equations representing neutral atmospheric conditions is solved. This calculation includes the Reynolds-averaged equations for motion (u_i), turbulent kinetic energy (k) and dissipation (ϵ) ($k - \epsilon$ model):

$$\frac{\partial \bar{u}_i}{\partial x_i} = 0 \quad (3.1)$$

$$\frac{\partial \bar{u}_i}{\partial t} + \bar{u}_j \frac{\partial \bar{u}_i}{\partial x_j} = \frac{\partial}{\partial x_j} K \frac{\partial \bar{u}_i}{\partial x_j} - \frac{1}{\rho} \frac{\partial \bar{p}}{\partial x_i} + \mu_{ij3} \cdot f \cdot (\bar{u}_j - u_{gj}) - C_D \cdot PAD \cdot |\bar{\mathbf{u}}| \cdot \bar{u}_i \quad (3.2)$$

$$\frac{\partial \bar{k}}{\partial t} + \bar{u}_j \frac{\partial \bar{k}}{\partial x_j} = \frac{\partial}{\partial x_j} K \frac{\partial \bar{k}}{\partial x_j} - \frac{\bar{u}_i \bar{u}_j}{\partial x_j} \frac{\partial \bar{u}_i}{\partial x_j} - \epsilon + c_{k1} \cdot C_D \cdot PAD \cdot |\bar{\mathbf{u}}|^3 - c_{k2} \cdot C_D \cdot PAD \cdot |\bar{\mathbf{u}}| \cdot k \quad (3.3)$$

where u_i is the wind vector with the components (u , v , w), x_i the spatial direction (x , z), at which the y -direction is not considered. K is the eddy viscosity and p the deviation from hydrostatic pressure. The third term on the right hand side of Eq. (3.2) describes the effect of Coriolis force, at which μ_{ijk} is used for the Levi-Civita symbol. The Coriolis parameter f for the study area is $1.13 \cdot 10^{-4} s^{-1}$. u_{gi} is the geostrophic wind component in i -th direction. The last term of Eq. (3.2) describes the absorption of momentum by drag force, whereas C_D is the drag coefficient and $|\bar{\mathbf{u}}|$ the magnitude of mean wind velocity. The turbulent character of the wind flow is regarded by the solution of Eq. (3.3) for the turbulent kinetic energy k (= TKE), where ϵ is the dissipation.

The drag coefficient was set constant to $C_D = 0.2$ for the whole forest, as in this first step the effect of the vegetation distribution on the wind flow should be evaluated only.

The values of the model constants for Eq. (3.3) were predefined with $\sigma_k = 1.0$, $c_{k1} = 1.0$ and $c_{k2} = 4.0$ and represent typical values (e.g. in JONES and LAUNDER, 1972). For closure of the set of equations, the eddy viscosity is derived from mixing length l with Eq. (3.4).

$$K = c_\mu^{1/4} \cdot l \cdot \sqrt{k} \quad (3.4)$$

where c_μ is a constant (here $c_\mu = 0.09$) that describes the squared ratio of the equilibrium shear stress to TKE. For the mixing length l an approach after QUECK and BERNHOFER (2010) was used:

$$l(z) = \min \left| \sqrt{(z - z_i)^2 + l_{p,z_i}^2} \right|, \quad z_i = [0, h] \quad (3.5)$$

where the mixing length $l(z)$ is calculated in vertical profiles for each horizontal grid index (the indexes i , j are omitted due to clarity). The distance to the nearest obstacle to position z is found by letting z_i go over the range of the canopy $[0, h]$. l_{p,z_i} describes the mean interelemental spacing at height z_i . This spacing is calculated

as follows:

$$l_{p,z_i} = \sqrt{\frac{ES}{PAD_{z_i} \cdot 1 \text{ m} + 10^{-9}} - ES} \quad (3.6)$$

where ES is a statistical parameter, which is derived from measured wind profiles (see QUECK and BERNHOFER, 2010). It characterizes the size of an average vegetation cluster and has typical values between 3.0 m^2 and 15.0 m^2 .

Even though only stationary conditions were investigated, the calculations were carried out in a time-dependent manner with a time step of 10 s. After the predefined simulation time of 36 hours, a stationary flow field was adequately established. All equations were solved at a fully implicit level. For every equation, convergence was fulfilled when the maximum relative change between two iterations was less than 0.0005. For every time step, all equations were solved repeatedly until the maximum, local divergence residuum decreased below 0.005.

3.6 Large-eddy simulation

For the presented large-eddy simulation (LES) study we restrict ourself to neutral atmospheric conditions. Additionally, variations in density and the influence of the Coriolis force can be neglected for the lower atmospheric boundary layer according to LUMLEY and PANOFSKY (1964). A LES distinguishes between the energy-carrying, resolved scales and the unresolved, sub-grid scales of motion to reduce the computational effort. This is accomplished by a filter operation ($\bar{\cdot}$) that, if applied to the Navier-Stokes equations, yields the resolved-scale or LES equations

$$\begin{aligned} \frac{\partial \bar{u}_i}{\partial t} + \frac{\partial (\bar{u}_j \bar{u}_i)}{\partial x_j} &= -\frac{1}{\rho} \frac{\partial \bar{p}}{\partial x_i} + \frac{\partial (2\nu \bar{S}_{ij})}{\partial x_j} + \frac{\partial \tau_{ij}}{\partial x_j} \\ &\quad + \bar{F}_{i,d} + \bar{F}_{i,p} \\ \frac{\partial \bar{u}_i}{\partial x_i} &= 0 \end{aligned} \quad (3.7)$$

where \bar{u} represents the resolved velocity, \bar{p} the resolved pressure, ν the kinematic viscosity ($1.46 \cdot 10^{-5} \text{ m}^2 \text{ s}^{-1}$ for air at 15°C) and $\bar{F}_{i,p}$ an uniform pressure gradient for maintaining a prescribed bulk velocity.

The effect of the subgrid-scales on the resolved scales of motion is represented by the so-called subgrid-scale stresses τ_{ij} (LILLY, 1967). They are related to the strain rate tensor (\bar{S}_{ij}) by using a Boussinesq approach

$$\tau_{ij} = 2K_r \cdot \bar{S}_{ij} - \frac{2}{3} \delta_{ij} \cdot K_r \quad (3.8)$$

with $K_r = c_v \ell_s \overline{k''}^{1/2}$ as sub-grid scale viscosity, which includes ℓ_s as the sub-grid scale mixing length. By this an incomplete set of equations is obtained. Hence, following DEARDORFF (1980) we additionally solve the

transport equation for the unresolved turbulent kinetic energy $\overline{k''}$ with some modifications for canopy flows according to SHAW and SCHUMANN (1992), an approach that was recently confirmed by SHAW and PATTON (2003). The interaction between the resolved scales and the vegetation is introduced to the LES equations (3.7) in terms of an aerodynamic resistance $\bar{F}_{i,d}$, which is calculated as the product of the local wind speed $|\bar{\mathbf{u}}|$, the projected plant area density PAD and an isotropic drag coefficient C_D

$$\bar{F}_{i,d} = -C_D \cdot PAD \cdot |\bar{\mathbf{u}}| \cdot \bar{u}_i. \quad (3.9)$$

Following SHAW et al. (1988) the drag coefficient is assumed to be $C_D = 0.15$, whereas the remaining constant $c_v = 0.0857$ is chosen according to SCHMIDT and SCHUMANN (1989).

The LES equations (3.7) and the subgrid-scale model are discretized by a semi-implicit, cell-centered finite-volume-method of second order accuracy. The model is implemented in the OpenFoam CFD toolbox in version 2.1 (JASAK, 1996; WELLER et al., 1998). Please refer to SCHLEGEL et al. (2012) for further details about the subgrid-scale model, the numerical method and the validation.

4 Parametrization

4.1 The vegetation structure

4.1.1 Resolution of the final laser scanner point cloud

Terrestrial laser scanners produce a huge number of 3D data points within a short time. Because of their hemispherical or panoramic scanning pattern, the resolution depends on the distance and may reach a point spacing from millimeters up to centimeters. Indeed, a reasonable scan resolution for the application at hand would be in the order of centimeters to allow for detecting small branch structures. Table 2 presents the characteristics of the laser scanning campaigns. ALS data are well suited for the determination of the digital terrain model and the canopy surface model. The mean point density of the available ALS data was 2 pts/m^2 . The final ALS and TLS data sets were merged together with a standard deviation of 0.25 m by using a RANSAC-based approach (see Section 3.2.3). Fig. 6 pictures the obtained TLS and ALS point clouds of a broad-leafed tree. A special feature of our data set are the additional laser scans from the top of the two towers, allowing for an improved documentation of the upper portions of the canopy.

4.1.2 Derived PAD from terrestrial laser scanning

The final voxel space derived from TLS, which was used in atmospheric boundary layer model (see Section 3.5) and large-eddy simulations (see Section 3.6) covers an



Figure 6: TLS point cloud of a broad-leaved tree in summer (left), autumn (middle) and ALS data of the same tree (right).

Table 2: Laser scanning campaigns from 2008 till 2011. *total number including previous campaigns.

	2008	2010	2011
Time	July	October	September
Phenology	leaf-on	leaf-off	leaf-off
Scan positions	8	6	11
Scan resolution	0.10 deg	0.10 deg	0.10 deg
Tower scanning	T4	T2	-
Laser scanner	Riegl & Faro	Riegl	Riegl
No. of points*	50×10^6	55×10^6	150×10^6
Area	190 m·60 m	190 m·60 m	330 m·170 m

area of $413 \text{ m} \times 253 \text{ m}$ with a constant grid resolution of 1 m (in all spatial directions). A finer voxel resolution would be possible, but would pose a severe burden to memory and computation time. As reported in QUECK et al. (2012), optical measurements tend to underestimate the *PAD* due to dense vegetation in the upper crown parts. In our case, the tower scans mitigated the problem and much of the occluded regions could be filled. As result we generated normalized point density in a voxel space of 1 m^3 resolution. Fig. 7 shows a profile (thickness 5 m) of the laser scanner point cloud, a color-coded voxel space with the number of hits and a voxel space of the normalized point density P_{total} of each voxel.

4.2 Parametrization of the drag force

4.2.1 The drag coefficient C_D – concept and current application:

In flow models the influence of vegetation on momentum is usually considered by extending the momentum equation with a friction term ($C_D \cdot PAD \cdot \bar{u} \cdot |\bar{u}|$). Thus,

a fine resolution of the *PAD* is a prerequisite for detailed flow modeling, and, as the turbulence parametrization is very sensitive in regards to the drag coefficient C_D , a proper definition of C_D is necessary. The C_D is a bulk coefficient and accounts for the geometry of the bluff body, the influence of surface texture, and, to some extent, the effects of viscous drag forces (see also MAHRT et al., 2001). It has been reported that the product of $C_D \cdot PAD$ decreases within closed canopies due to sheltering (e.g. THOM, 1971) and that C_D depends on wind velocity due to the streamlining of elastic roughness elements (RAUPACH and THOM, 1981; BRUNET et al., 1994; FINNIGAN, 2000). However, C_D is also designated as the most uncertain parameter in making estimates of momentum fluxes (ARYA, 2001). For the sake of simplicity and due to the lack of information, commonly constant C_D (between 0.1 and 0.4) are applied in numerical flow models (e.g. SHAW and SCHUMANN, 1992; GROSS, 1993; YANG et al., 2006; FRANK and RUCK, 2008; DUPONT et al., 2011). This simplification was also applied to the numerical simulations within this study yet.

4.2.2 The variable drag coefficient C_D

Within *TurbEFA* the topics streamlining and sheltering were already addressed in QUECK et al. (2012) and are summarized in the following. Neglecting the minor terms in the momentum equation (Coriolis force, buoyancy effect, advective transport, the pressure gradient, dispersive fluxes), profiles of the drag coefficient C_D were defined by the equilibrium between the vertical change of drag force (left hand side of Eq. 4.1) and the rate of horizontal momentum transfer (right hand side of Eq. 4.1).

$$\rho \frac{d\overline{u'w'}}{dz} = -\rho \cdot C_D \cdot PAD \cdot \bar{u} \cdot |\bar{u}| \quad (4.1)$$

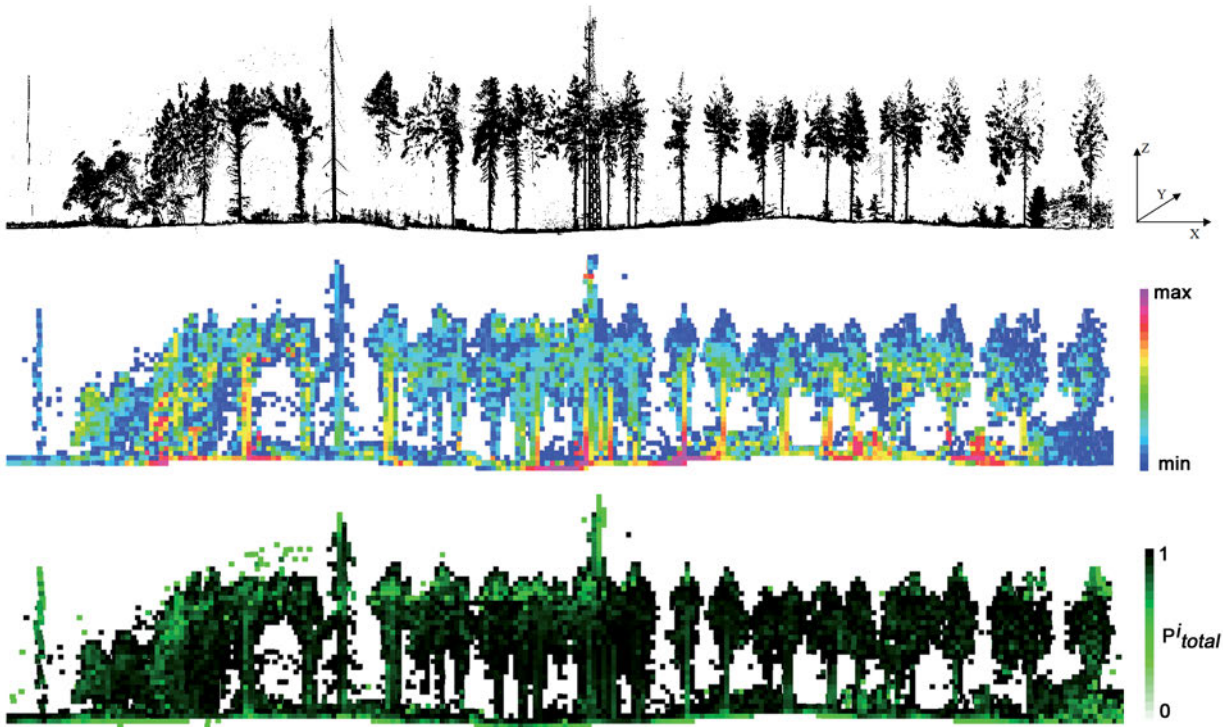


Figure 7: A segment of the model domain with a depth of $\Delta Y = 5$ m and a length of $\Delta X = 225$ m, including tower T2, T3 and T4: point cloud (top); 1 m voxel space with color-coded point numbering n_{nit} , increasing number from blue to purple (middle); 1 m voxel space with a normalized point density P_{total} (bottom).

where ρ is the air density and $|\bar{\mathbf{u}}|$ is the magnitude of mean velocity. The product $C_D \cdot PAD$ was then computed from wind measurements by rearranging Eq. (4.1). Using the laser derived PAD distribution and multi-level high-frequency wind velocity measurements, we analyzed the behavior of the C_D at different positions at the *Fluxnet* tower T4 and for different wind conditions.

Results from the experiments *WinCanop* (in 2007) and *TurbEFA* (5/2008 to 4/2009) were considered. Despite the different periods in time and slight changes in sensor positions, the calculated local drag areas reveal conforming patterns and affirm repeatability.

A strong dependency of C_D on the wind velocity (or streamlining) was observed for the topmost layers of the canopy for westerly winds. However, for winds from south and east and the deeper layers of the canopy we see only a weak or no correlation between C_D and the wind velocity. As Fig. 1 shows the fetch for the winds from west and north is much shorter (about four times the canopy height h) as the fetch from south and east. Equation (4.2) can be used to integrate the measurements vertically to an average drag coefficient C_{Da} .

$$C_{Da} = \left(\int_{z=0}^h PAD \cdot \frac{\bar{u}^2}{u'w'} dz \right)^{-1} \quad (4.2)$$

Additionally to the analysis in QUECK et al. (2012) we calculated C_{Da} for all wind directions and plotted it against the wind velocity in Fig. 8. The reaction of the

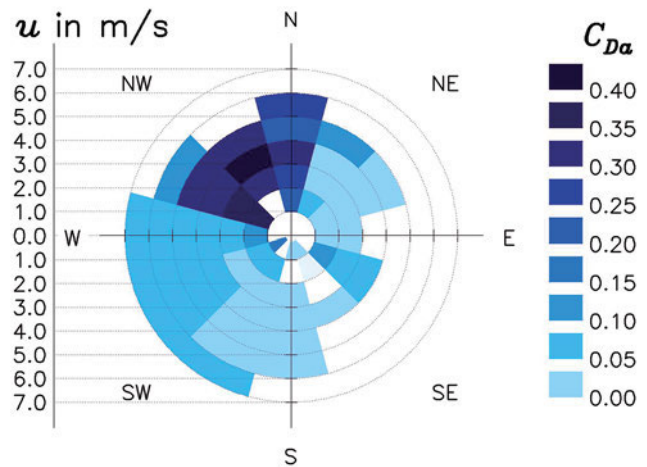


Figure 8: Wind dependence of the vertical averaged drag coefficient C_{Da} . White sectors contained not enough data for statistical analysis.

canopy as a whole shows no clear dependence. Whereas we observe the highest C_{Da} in the lowest wind velocity class mostly (except the three north wind sectors), there is sometimes an increase of C_{Da} during high wind velocity too. We conclude that C_D depends on wind speed for the topmost layers and for single trees, but the effect of this dependence on the drag force exerted by the whole canopy is only small. Much more impressive is the strong increase of C_{Da} for winds from west-north-

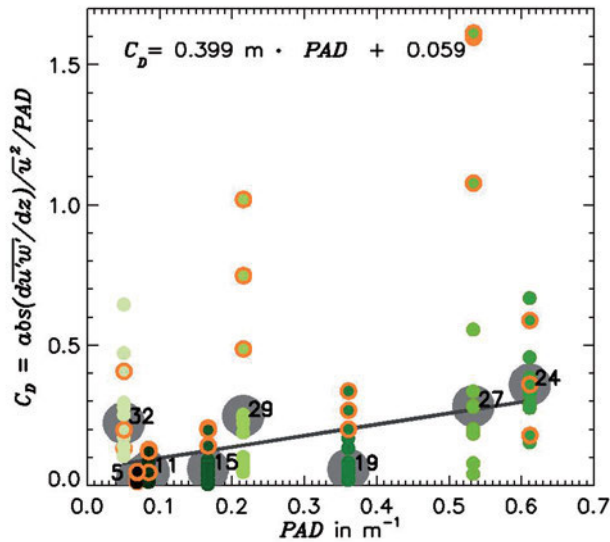


Figure 9: Influence of the plant area density and plant structure on the C_D . Small circles show the C_D for single wind sectors, the big circles give the median over all wind sectors. The green shading indicates the measurement level, which is also given in meters by the numbers beside the big circles. The three 30° wind sectors west-north-west, north-north-west and north are marked by black encircled symbols. The gray line shows the regression of C_D on PAD as well as the equation.

west and north. Either the forest clearing or the small hill ‘S-Berg’ seems to increase the turbulent transport of momentum in the forest. Thus, edge effects (DUPONT et al., 2011), i.e., the importance of the neglected terms of the momentum equation, have to be considered for this wind sectors. The definition of the stand volume and the respective PAD in Eq. (4.1) is also a source of uncertainty, which influences the measurements at a certain point (see QUECK et al., 2012).

A closer view reveals, that the high C_D values are obtained for the topmost canopy layers only (see Fig. 9). Regions of enhanced turbulence in the lee of the forest edge (RAUPACH et al., 1987; DUPONT and BRUNET, 2009) might cause an increase of the kinematic stress, which is counterbalanced not only by the drag force.

Contrary to the assumption of a shelter effect, the calculated C_D in Fig. 9 revealed an increase of C_D with PAD . The strength of this dependence changes with wind direction, but shows the similar pattern for directions with a fetch of four times the canopy height (h) as for those with a fetch of more than $10 h$. The regression of the PAD to the mean C_D over all wind directions results in a slope of 0.4 m and an intercept of 0.06 . The observed dependence on PAD could most likely be attributed to specific plant structures. We assume, a higher PAD is related to more separated surfaces (imagine a volume with twigs and leaves compared to one containing a stem or branches) and, therefore, it exerts a higher drag on the flow.

5 Model results: sensitivity on parametrization, closure and sub-grid model

5.1 Wind tunnel

5.1.1 Influence of the tree models on the vertical profiles

To assess the suitability of the two different tree model types we build two homogeneous vegetation models of 35 cm length (imitating 150 m in reality). Fig. 10 shows that the profiles of both models match the field experiment above the canopy indicating comparable flow conditions. Nevertheless, within the canopy the shape of the profiles is different. The conventional tree models fail to reproduce the strong deceleration within the crown space as well as the secondary velocity maximum within the trunk space.

5.1.2 Development of the mean velocity over the measurement transect

Mean velocities were measured with HDA in vertical profiles from 1 mm to 120 mm with steps of 1 mm . These heights correspond to profiles between 0.45 m and 54 m and steps of 0.45 m in the field. Fig. 11 shows a wind field, which was derived by interpolation between 17 measured profiles along the transect of the towers.

The profiles on the clearing show that the momentum is transported downwards fast behind the leeward forest edge (regarding the defined incident flow direction from west). The lower layers appear to be separated from the flow above for a short distance from the edge only. The second half of the clearing is characterized by very straight, almost linear wind profiles. They still reflect the attenuation of the horizontal velocity due to the surrounding canopy but show the momentum entrainment into the open space of the clearing already.

The isotachs within the canopy demonstrate an increasing adaptation of the flow to profiles dictated by the in-canopy impulse budget. Starting from the forest edge the flow within the canopy is continuously decelerated, whereas the velocity within the trunk space reveals almost no horizontal gradient. As a result we observe a strong velocity gradient at the top of the canopy and a small secondary velocity maximum within the trunk space behind the *Fluxnet* tower (T4).

5.2 Averaged boundary layer model HIRVAC-2D

Investigating the effect of a refinement of the vegetation model we applied a simplified homogeneous plant area distribution (HOM) and a complex plant area distribution (HET, derived from laser scanning). The computational domain ($x_D = 2 \text{ km}$, $z_D = 2 \text{ km}$) is aligned along the transect delineated by the measurement towers. The

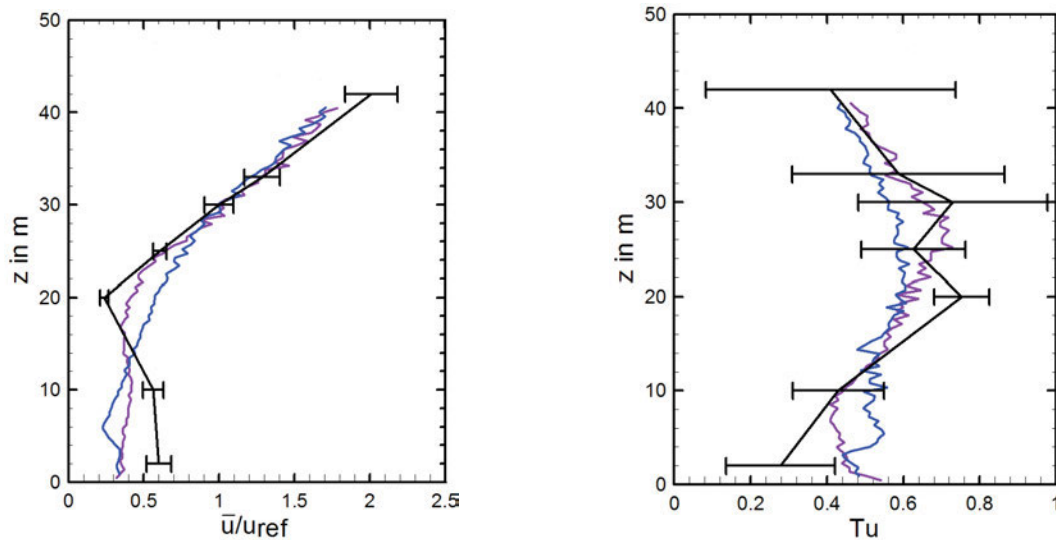


Figure 10: Profiles of wind velocity (left) and turbulence intensity (right), from field measurements and from wind tunnel measurements. The black line with whiskers shows mean and standard deviation of the field measurements at T4. The canopy build wire mesh (purple line) generates better fitting profiles than that build by conventional tree models (blue line).

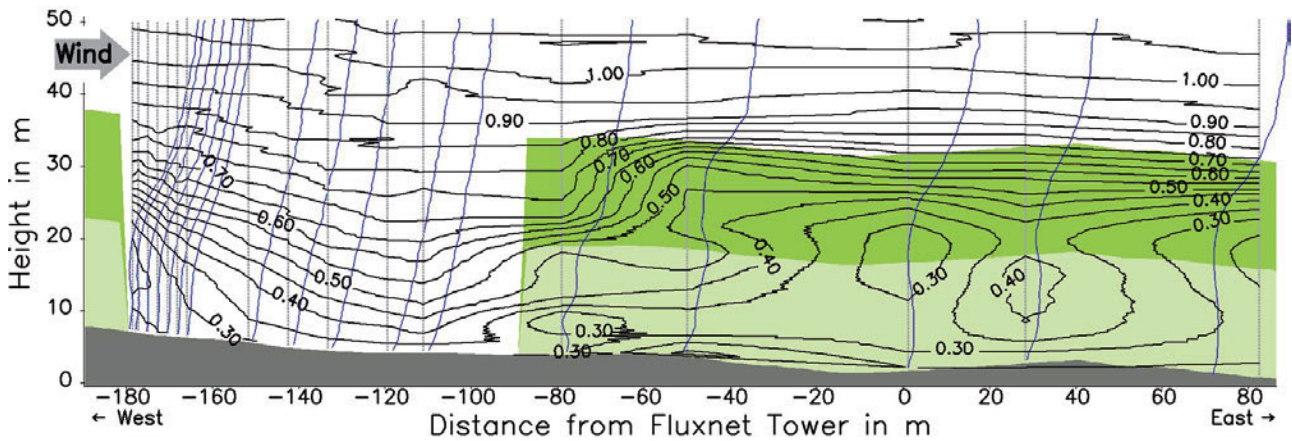


Figure 11: Contour plot of the horizontal velocity within the wind tunnel derived from measured profiles (at the dotted lines) applying a Delaunay triangulation, all measured velocities are normalized with the velocity at $x = 0\text{ m}$, $y = 0\text{ m}$ and $z = 42\text{ m}$. The vertical profiles of the velocity (blue lines) are supposed to illustrate the profile shape and have no scale. The green shading in the background indicates the wire frame canopy model.

model worked on a rectangular grid with number of grid points of 245 horizontally and 150 vertically. The vertical grid size followed a geometric series. At the ground, a minimal grid size of $z_0 = 0.1\text{ m}$ was assumed. With height, the grid distance increased by a constant factor to a maximum thickness of 50 m at the upper model domain. Within the crown space, the vertical distance between grids was about 1 to 2 m. About 60 vertical layers are used to calculate the stream flow under the influence of the forest canopy. The horizontal grid size is $\Delta x = 1\text{ m}$ within the range $x = [-180, 10]$ (relative to the base of T4). The range covers the forest clearing and the measurement towers. Within the periphery of the domain the horizontal grid size increases and reaches $\Delta x = 80\text{ m}$. Periodic boundary conditions were applied in horizontal direction. For the planar upper boundary we imposed

free-slip conditions and no-slip condition for the lower boundary. The flow within HIRVAC-2D was driven by a geostrophic wind speed of 20 m/s, which generates a wind velocity of around 4 m/s at the reference position (T4, $z = 42\text{ m}$). The difference of the surface roughness in both vegetation models creates slightly different velocities at this point. For the comparison with other results the velocities were normalized to match 4 m/s at the reference position.

In Fig. 12, the horizontal gradient of wind speed reaches a maximum at the upper forest edge of the homogeneous forest canopy. This fact is primarily due to abrupt transition from a vegetation-free atmosphere to the highest amount of PAD of the homogeneous forest leading to a strong increase of the form drag $-C_D \cdot PAD \cdot |\bar{\mathbf{u}}| \cdot \bar{u}_i$ as shown in Eq. (3.1).

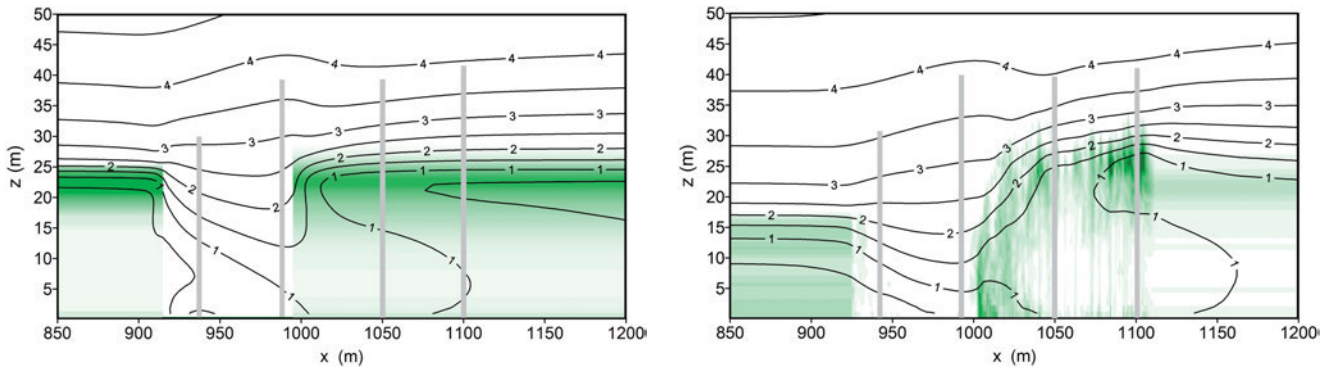


Figure 12: Isotachs of the horizontal wind velocity (in m/s) calculated with HIRVAC-2D for the homogeneous (left figure) and the heterogeneous vegetation model (right figure) along the measurement transect. The green shading denotes the *PAD*.

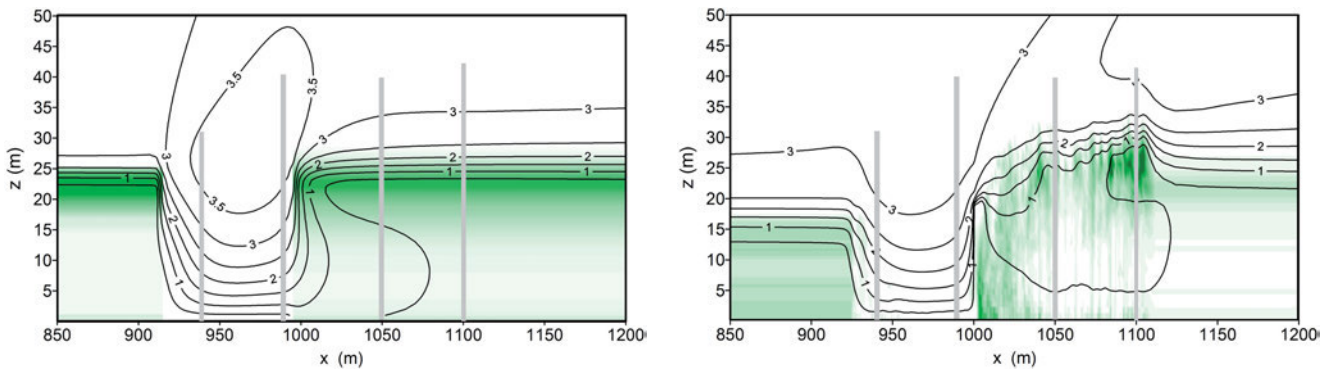


Figure 13: Contour plot of the TKE (in m^2/s^2) calculated with HIRVAC-2D for the homogeneous (left figure) and the heterogeneous vegetation model (right figure) along the measurement transect. The green shading denotes the *PAD*.

In case of TKE (k) the interaction between the *PAD*-dependent production and the dissipation $c_{k1} \cdot C_D \cdot \text{PAD} \cdot |\bar{\mathbf{u}}|^3 - c_{k2} \cdot C_D \cdot \text{PAD} \cdot |\bar{\mathbf{u}}| \cdot k$ (see Eq. 3.3) leads to local maximum of TKE above the clearing, and afterwards, in context with a rapid decrease of velocity, to a fast decline of TKE in the crown space of the forest canopy.

The relatively open trunk space opposes less form drag and a slighter decline of velocity and TKE.

The model run using the heterogeneous vegetation distribution leads to more variable horizontal gradients of wind velocity and a heterogeneous TKE distribution.

The forest edge of heterogeneous vegetation model is composed more gradually, which permits a better penetration of flow into the inner crown space of the forest. This leads further to a shift of the TKE maximum in wind direction compared to the homogeneous forest where the TKE maximum is located over the clearing.

In contrast to the homogeneous canopy the laser detected trunk space includes areas of both very low and relatively high *PAD*. As a result, the contrast between wind speed outside and inside the forest is weaker as for the homogeneous canopy. However, the high *PAD* at the forest edge lead to a sharp gradient of TKE from the clearing to the inner forest. This fact is mainly due to the strong interaction between TKE and *PAD* in the mixing length parametrization (Eq. 3.3).

Fig. 14 demonstrates that the usage of the detailed vegetation model leads to an improvement of the wind profile simulation at the location T3 in relation to the measurements. Especially in the trunk space (low *PAD*) the simulated wind profile coincides much better with the measured profile in comparison to a homogeneous *PAD* distribution (left figure). At the location of *Fluxnet* tower (T4 right figure) the real *PAD* distribution is more homogeneous, and the model performance was not changed significantly by replacing the homogeneous *PAD* distribution with real *PAD* measurements.

5.3 Large-eddy simulation

A series of LES studies was performed for a computational domain of $600 \text{ m} \times 600 \text{ m}$, containing the field site in its center. To assess the importance of various modeling aspects we considered four different scenarios: In the simplest case, referred to as HOM-Flat, we assumed the vegetation to be horizontally homogeneous within each forest plot and neglected all variations in the ground height, resulting in a flat terrain model (Fig. 15(a)). The *PAD* for this case is derived from observed statistical data for mean tree height, mean PAI using generic profiles for the plant area density (PETERS and EIDEN, 1992; KRAUS, 2008).

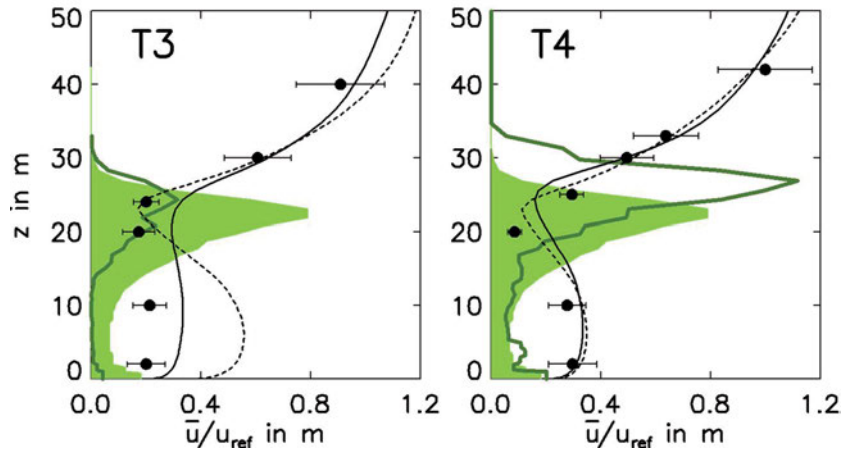


Figure 14: Normalized profiles of the horizontal velocity calculated with HIRVAC-2D at the two tower locations within the forest. The model results using the heterogeneous vegetation model (straight lines) reveal a better agreement with the field measurements (filled circles with whiskers), than that using the homogeneous vegetation (dashed lines) at the forest edge. The green filled area and the thick green line indicated the *PAD* of the homogeneous and heterogeneous vegetation model respectively.

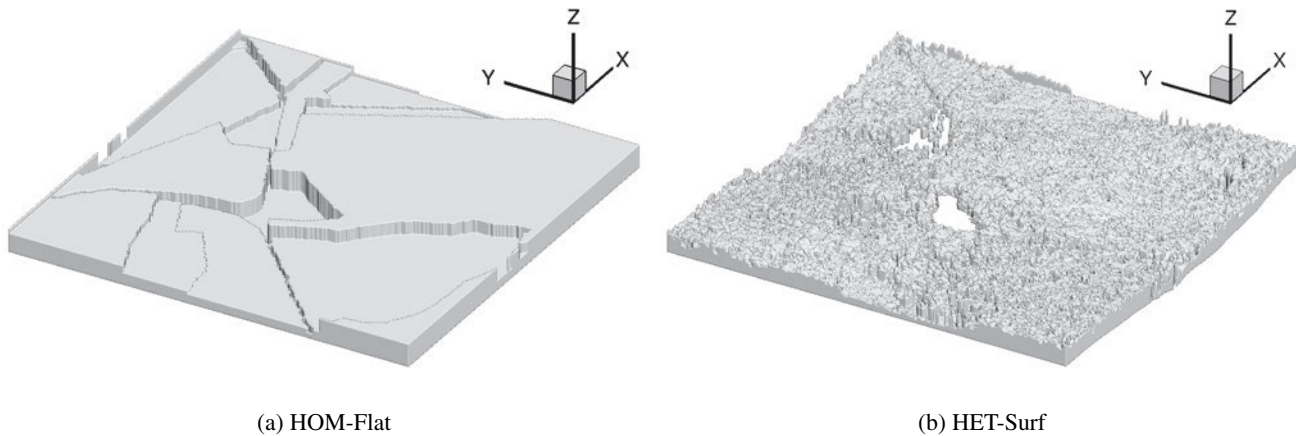


Figure 15: Plant area distribution and topography for the simplest (a) and most comprehensive (b) scenarios used in the LES study.

Case HET-Flat is based on the same terrain model, but employs a three-dimensional, heterogeneous *PAD* that was obtained from TLS in the central region ($328\text{ m} \times 172\text{ m}$) and from the virtual canopy generator in the periphery.

For scenarios HOM-Surf and HET-Surf we used the same *PADs* as in HOM-Flat and HET-Flat, respectively, combined with a high-resolution terrain model. This model fits to the ATKIS[®]-DGM2 data in the central region, but was modified in the peripheral region to allow for periodic boundary conditions in the horizontal directions (for details please refer to SCHLEGEL et al., 2014). As an example, Fig. 15(b) shows the *PAD* and the topography for case HET-Surf.

In the vertical direction, the computational domain extends to 240 m above the highest point on ground, giving a planar upper boundary, for which free-slip conditions were imposed. Finally, a no-slip condition with the logarithmic law for rough walls was applied to the bottom.

As a consequence of topography the computational mesh becomes non-orthogonal and non-equidistant for HET-Surf and HOM-Surf. Applying an average spacing of approximately 2 m yielded 302×200 grid cells in the horizontal directions and between 120 and 132 in the vertical direction. For HET-Flat and HOM-Flat a constant mesh-spacing of 2 m was used.

Note that the grid cells and the voxels defining the *PAD* generally do not coincide. Therefore, we calculate the mean value of the *PAD* over those voxels, whose center points are located inside a given grid cell.

To obtain a flow regime comparable to the field measurements, the meso-scale pressure force $\tilde{F}_{i,p}$ was adjusted to achieve a mean velocity of approximately 4 m/s at a height of 42 m above ground at tower T4. Time integration was performed over a period of 11 100 s with a time step of 0.1 s. For calculating the mean values and fluctuations we used snapshots that were sampled at a rate of 0.5 Hz over the last 3 600 s of the computational run.

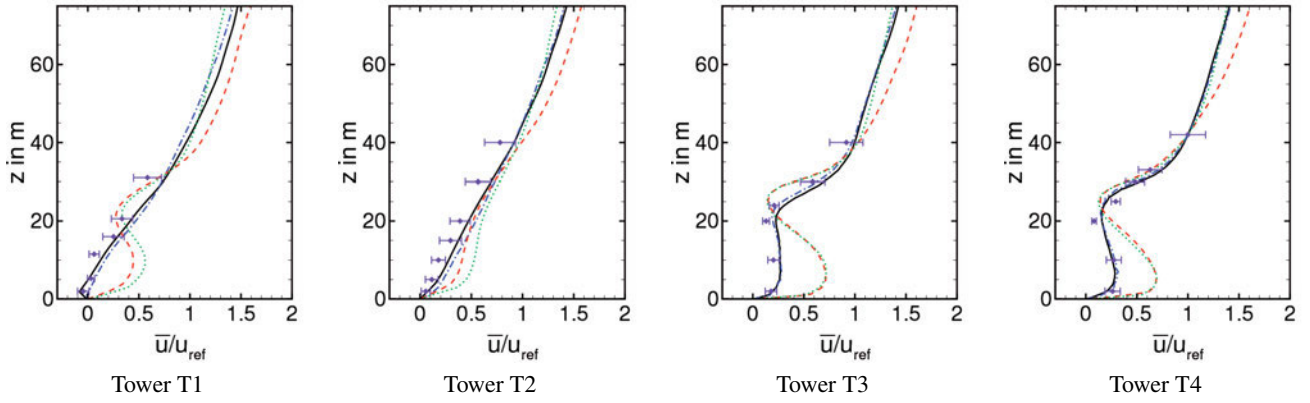


Figure 16: Comparison of the mean streamwise velocity \bar{u} between the four large-eddy simulations HET-Surf (black solid line), HET-Flat (blue dashed-dotted line), HOM-Surf (red dashed line) and HOM-Flat (green dotted line) and the field experiment (purple diamond symbol) at the position of the measurement towers. For the results of the large-eddy simulation the velocities denote filtered quantities.

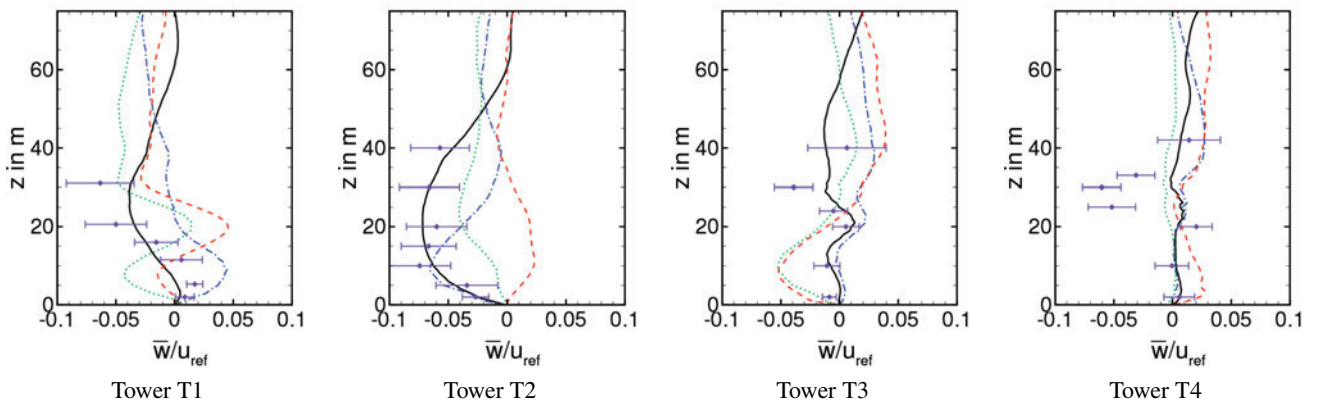


Figure 17: Comparison of the mean vertical velocity \bar{w} between the four large-eddy simulations HET-Surf (black solid line), HET-Flat (blue dashed-dotted line), HOM-Surf (red dashed line) and HOM-Flat (green dotted line) and the field experiment (purple diamond symbol) at the position of the measurement towers. For the results of the large-eddy simulation the velocities denote filtered quantities.

Fig. 16 compares the computed profiles of mean streamwise velocity with corresponding field data at the tower positions. Both scenarios featuring piecewise homogeneous forest plots (HOM-Flat and HOM-Surf) show severe qualitative and quantitative deviations from the measurements. Especially near the ground the wind speed is considerably overestimated. The S-shape of the profile is overemphasized at towers T1, T3 and T4. In contrast, simulations HET-Flat and HET-Surf fit nicely to the field data at all positions. However, at T1 only HET-Surf succeeds in reproducing the weak recirculation zone observed in the experiment. While the influence of topography appears to be marginal in the streamwise velocity, its effect becomes more pronounced for the vertical component. Fig. 17 reveals a remarkable agreement between HET-Surf and the measurements at towers T1–T3. HET-Flat achieves considerably less accurate, but yet reasonable results, while HOM-Flat and HOM-Surf fail substantially. At tower T4, the field data indicate a weak downward flow in the crown section, which has no counterpart in the simulations. As an example of turbulent statistics, Fig. 18 shows the computed and measured profiles of the normalized Reynolds

stresses $\overline{u'w'}$. Again, both cases assuming piecewise homogeneous vegetation achieve only poor agreement, while HET-Surf fits excellently and HET-flat still reasonably to the field data.

In summary, the presented results show consistently that the heterogeneous vegetation structure and the topography must be both resolved to obtain reliable results in micro scale LES of canopy flows.

6 Turbulent flow over the clearing - inferred from measurements and numerical simulations

6.1 Survey

In this section a combined view on the results of the measurements and simulations is used to investigate the flow disturbance caused by the clearing. Firstly, we compare the final results of the wind tunnel measurements, the boundary layer modeling and large-eddy simulation with the meteorological field measurements by means

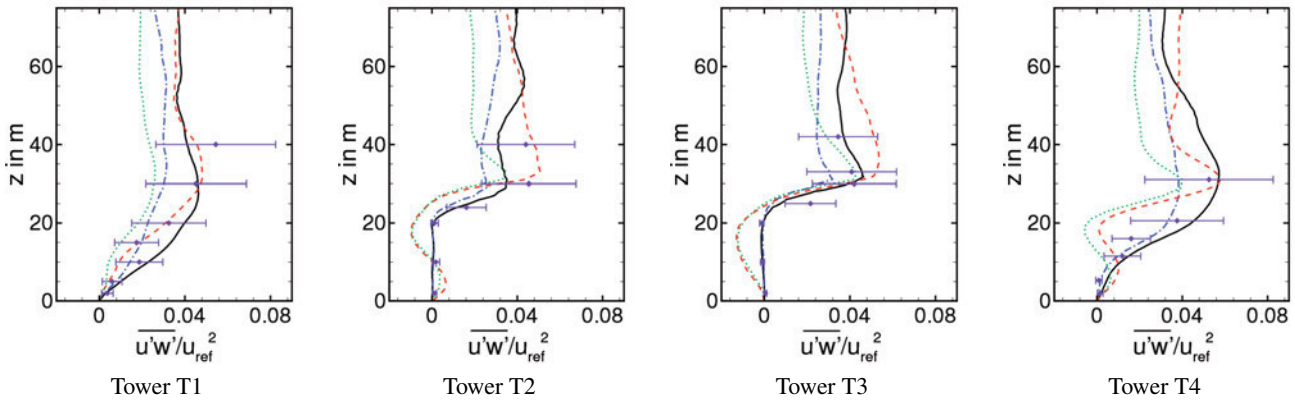


Figure 18: Comparison of the Reynolds stress $\overline{u'w'}$ between the four large-eddy simulations HET-Surf (black solid line), HET-Flat (blue dashed-dotted line), HOM-Surf (red dashed line) and HOM-Flat (green dotted line) and the field experiment (purple diamond symbol) at the position of the measurement towers.

Table 3: Conditions for the standard case measured at T4 in $z = 42$ m. ζ is defined by z/L (where L is the Monin-Obukhov length).

Stability	$-0.1 < \zeta < 0.1$
Wind direction	$255^\circ < WD < 285^\circ$
Wind velocity	$2 \text{ m/s} < u < 4 \text{ m/s}$

of vertical profiles of statistical quantities. Secondly, we discuss the flow fields calculated by the numerical simulations looking for the adjustment to the changing surface and the partitioning between local disturbances and long range effects of topography.

6.2 Comparison between field measurements, wind tunnel and numerical models

Comparing field measurements and model results, we defined a standard situation for the reference position at *Fluxnet* tower T4 in a height of 42 m. It is characterized by winds from west, wind velocity around 4 m/s and neutral stratification. Table 3 gives the ranges for the selection of the field measurements. During the *TurbEFA* experiment we recorded field data over 7550 hours. Applying the constraints in Table 3 128 hours were selected (i.e., the statistics of 256 half-hourly data sets) for the comparison. The Figs. 19, 20 and 21 show the ensemble means of these measurements as well as the standard deviation as error whiskers. The driving forces within the models were adjusted so that the simulations match standard case at the reference position.

The effect of the different model parametrizations was discussed in the Sections 5.2 and 5.3. In accordance, the results of the numerical models point to a significant improvement using a refined vegetation parametrization. In Figs. 19 and 20 we compare the respective best results of the different approaches with the plots of normalized wind velocity, turbulent kinetic energy and Reynolds stress. In the following the abbreviations BLM and LES refer always to the simulations using the heterogeneous vegetation model (for the LES the case HET-Surf).

The wind velocity is discussed by considering the great importance not only for the quantification of the force affecting the trees, but also for the advective fluxes of scalars, which cause still a remarkable uncertainty determining the exchange of mass and energy between forests and the atmosphere. The TKE is selected as an integral criteria of how well the simulations reflect the development of turbulence, which is a precondition to reproduce the turbulent fluxes within the model domain. Within the WT experiment an one dimensional *Hot Wire* anemometer was applied, therefore no vertical wind, TKE and Reynolds stress could be measured. The TKE for WT was approximated utilizing the standard deviation of the velocity.

Looking at the FM results (\overline{u}/u_{ref} , but also $\overline{u'w'}/u_{ref}^2$ and *TKE*) it can be distinguished between two general shapes of the profiles: ‘S’-shaped forms within and above the forest stand and more or less linear profiles over the clearing. The stand profiles are composed of a flow above the canopy, which is characterized by a logarithmic velocity profile, and a flow within the canopy, whose velocity exceeds the vertical momentum transfer. The inflection point in the profiles at canopy top marks the layer with the strongest wind shear between the coflowing streams. These features are well-known (see RAUPACH et al., 1996; FINNIGAN, 2000, for an overview), although, the reasons for the secondary velocity maximum within the trunk space have not yet been fully elucidated. Comparing the TKE and \overline{u}/u_{ref} profiles we see a fundamental difference between the coflowing air streams. The turbulence within the trunk space is much lower than that above the canopy. Additionally, the increase of \overline{u}/u_{ref} between T3 and T4 indicates a non-turbulent source of momentum for the flow within the trunk space.

Both numerical models retrieve the stand profiles well, even though the velocity is somewhat overestimated by the BLM. The WT model produces a higher velocity and turbulence within the canopy, which is probably caused by the far more simplified vegetation model.

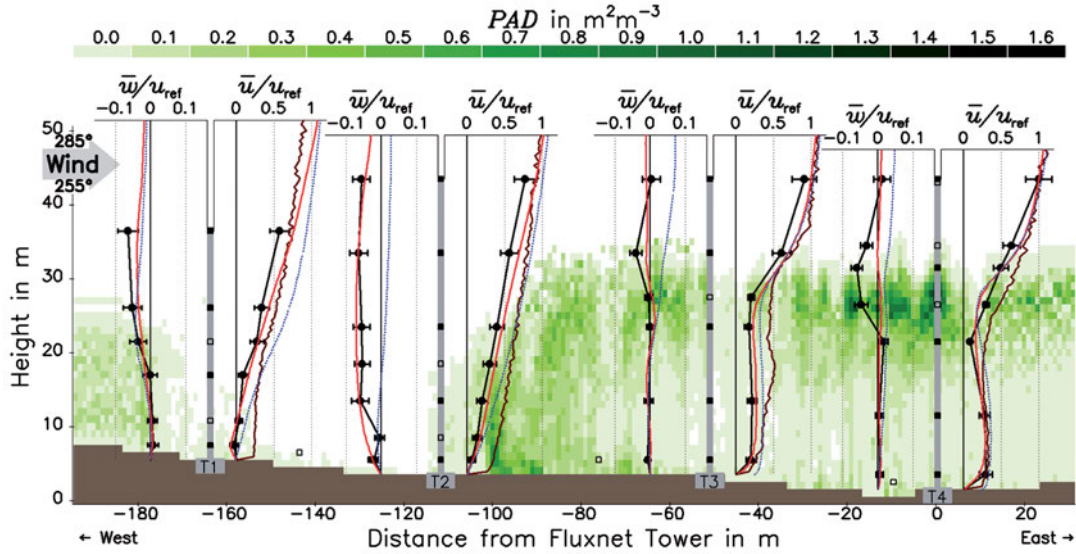


Figure 19: Profiles of the vertical and the horizontal wind velocity at the tower positions. The filled circles with whiskers show the field measurements. The wind tunnel results (dark brown line, only available for \bar{u}/u_{ref}) are not smoothed and exhibit the scatter of the single measurements by the zigzag course. The BLM results (dotted blue line) deviate somewhat from the measurements, especially from the vertical wind at T2. The best result is gained from the LES (straight red line). The sensor positions are depicted by black squares (filled squares were operated permanently and open squares temporarily), the towers by gray bars and the green shading depicts the PAD from TLS measurements (averaged over 30 voxel in north-south direction).

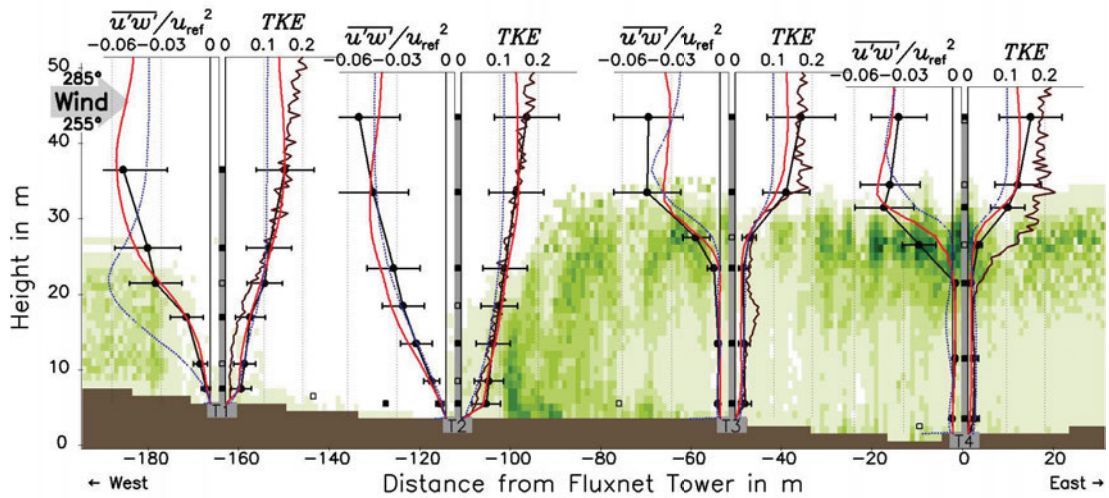


Figure 20: Profiles of the turbulent kinetic energy (TKE) and the normalized Reynolds stress $\overline{u'w'}/u_{ref}^2$. Color indications and symbols are the same as in Fig. 19 (FM: filled circles with whiskers, WT: dark brown line, BLM: dotted blue line, LES: straight red line).

The vertical velocity profiles deviate between all approaches. However, they show similar shapes for T3 and T4. For both positions, the FM observes negative \bar{w} at the upper layers of the canopy and slightly positive \bar{w} below the canopy. The first might be overestimated as the flow is intensified within the gaps between the tree crowns (where sensors are commonly positioned). The LES shows very small \bar{w} , but also a convergence within the canopy, with slightly negative \bar{w} in upper layers of the canopy and positive \bar{w} in the lower layers. In contrast to the results of the LES, the BLM simulates pos-

itive \bar{w} over the whole canopy probably caused by too much horizontal advection from the forest edge.

The profiles on the clearing show a transition from stand profiles to profiles over a lower vegetation. This process was already described by RAUPACH et al. (1987). It is dominated by a downward transport of turbulence, which is shown by the concordant TKE profiles of all approaches at T2. The size of the clearing (only $\approx 2-3$ h) seems to be sufficient that stronger turbulence from above the canopy reaches the ground of the clearing at tower T2. Despite the proximity to the forest edge

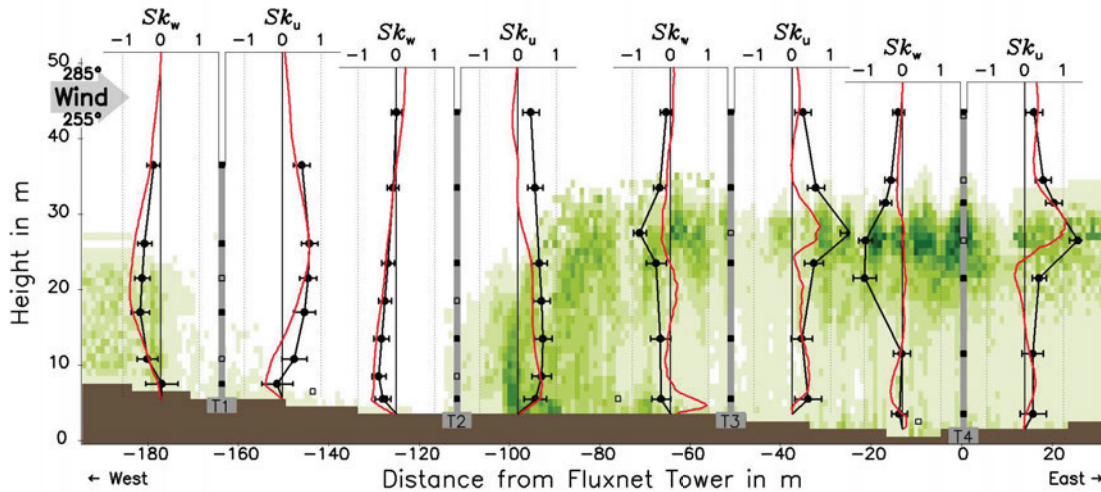


Figure 21: Profiles of the skewness of the horizontal streamwise velocity and of the vertical velocity. The filled circles with whiskers show the field measurements and the red lines the LES results.

and the low horizontal velocity, the lower layers at T1 show a higher TKE than that within the trunk space around T3 and T4. The intensification of turbulence is obviously caused by vertical movements in the separation zone as the horizontal wind velocity is close to zero. An exception is the WT experiment, where the TKE at T1 is low and comparable the TKE within the canopy. This might be caused by the more homogeneous canopy of the WT model, with higher horizontal velocities in the lower layers. Thus, a separation zone develops hardly. Despite that, the TKE increases between T1 and T2 within the WT and matches results of the other approaches there.

The mean wind velocities follow a complicated pattern, which can not be presented here in detail. We observe a different flow pattern between low wind velocities and stronger winds. Stronger winds are able to penetrate the windward forest edge near T2, whereas weaker winds ($u_{ref} < 1$ m/s) are redirected and cause a local recirculation on the clearing.

The reversal flow reaches up to a height of 10 m, but shrinks with increasing wind velocity. Investigating the averaged velocities, the recirculation is still revealed by the turning back of the horizontal velocity and the positive vertical velocity at the lower layers around T1 (see also Fig. 17a) as well as the negative vertical velocity at T2 (Fig. 17b). However, the height of the reversal flow has shrunk to $h/5 \approx 5$ m. Considering the intermittent nature of the turbulent flow we assume that the recirculation is the more frequent case and only the stronger gusts are able to enter the trunk space.

The recirculation within the separation zone behind forest-clearing transitions was observed in several studies for homogeneous forest stands (e.g. FRANK and RUCK, 2008) or for bigger clearings (DETTO et al., 2008; CASSIANI et al., 2008). A new feature is the influence of the windward edge on the flow, which is even more

obvious for the lateral wind components as shown in SCHLEGEL et al. (2014). This is different to RAUPACH et al. (1987) where no influence of the forest edge upward the flow on the clearing was observed.

Both the BLM and the WT overestimate the wind velocity on the clearing. The BLM is able to reproduce the TKE profiles, but fails to retrieve the effect of the turbulent motions within the separation zone (i.e., the recirculation). Furthermore, the two dimensional setup of the BLM does not consider the lateral wind component. Both handicaps lead to an overestimation of the mean momentum entering the forest from the clearing. A similar effect, but with another reason is observed for the WT. There the vegetation model is more ventilated in general, as a result no separation zone develops and high horizontal wind velocities are measured at T2. A low Reynolds number could be another reason for the absence of the separation zones. The viscous forces are too strong compared to the inertial forces and prevent the recirculation. Thus, the scale of 1:450 was chosen too high to reflect the processes on the forest clearing. We can conclude that to resemble the complex flow around a typical forest clearing a three dimensional simulation is necessary and that the accuracy of the results depends strongly on the vegetation model.

The application of a PAD dependent C_D in future runs of the BLM and the LES would increase the drag force exerted by the forest edge and the top canopy layers on the air flow. Presumably, the enhanced roughness would stretch the wind profile above canopy at T4 and slow down the velocity within and around the canopy. This would still improve the results of the numerical simulations. The process of the forest edge penetration would be affected especially.

6.3 Adjustments to vegetation structures

The adjustment of the turbulent flow to forest inhomogeneities has been studied by many authors during the last decades. LEE (2000) gives an review, BELCHER et al. (2003) schematized seven different regions across a forest canopy and among others DETTO et al. (2008) and DUPONT et al. (2011) discuss the subject as a background for the interpretation of field measurements and LES. For the flow crossing a small clearing it can be distinguished between six regions: at the clearing we look for an *exit region* at the leeward forest edge and for an *impact region* at the windward forest edge, then within the canopy for the *adjustment region* and further downstream a balance or *canopy interior* region, then above the canopy a *roughness layer* and above this an *internal boundary layer*.

The clearing *Wildacker* is obviously too small to develop an independent *exit* and *impact region*. BELCHER et al. (2003) defines a streamwise length scale of $h\bar{u}_h/u_*$ to fill the velocity deficit in the wake after the forest-clearing step. Whereas we assume that the development of the *impact region* is influenced by the wind velocity \bar{u}_h , but also the *PAD* (beside the geometry of the forest edge). The wind pattern on the clearing varies from a direct flow through to recirculation, as it was observed in an early work of RAUPACH et al. (1987) too.

The linear velocity profiles and the intense turbulence over the clearing shown in Fig. 19 and 20 might be described by the existence of a *mixing zone* at the top of the *exit region*. LEE (2000) assumes a region where the two coflowing streams from above and from within the canopy (probably causing Kelvin-Helmholtz instabilities) generate enhanced turbulence and vertical momentum transport. The strong coupling accelerates the air within the clearing.

Another feature are the downward tilted velocity vectors over the clearing shown in Fig. 22. They point almost orthogonal to forest edge despite the relative high *PAD*. Neither the LES nor the FM show signs of a separation zone before the windward forest edge. Above the following canopy we found a slightly increased velocity, but in parallel to the canopy top. Within the crown space we identified undulating winds with a fast decreasing horizontal velocity component. In contrast, we observe a slightly accelerating horizontal velocity within the trunk space after a depression behind the edge. The vertical exchange within the trunk space seems to cease almost completely as both the average vertical velocity and the turbulent exchange are low (see Fig. 20). Fig. 19 shows an increasing velocity difference between the canopy air and the trunk space air, which results in a small turbulent momentum flux upwards at T4 (Fig. 20). This development is inverse to the process described in DUPONT et al. (2012), but it may be typical as closed forest edges followed by heterogeneous canopies appear frequently.

The LES designates very clear regions with lateral velocities in Fig. 22. Note, the velocities are still very small at the transect position (about 3 % of the reference

velocity at the top of T4). Thus, in reality and within the field measurements such a clear picture cannot be found. However, SCHLEGEL et al. (2014) showed that the transect is just the origin of a developing north-eastward flow along the clearing.

The two coflowing air streams are mixed over the clearing and the forest edge. The adjustment of the mean flow to the stand in the lee of the clearing is marked by the ‘S-shaped’ profiles of the horizontal wind velocity, which occurs at T3 already. The adjustment of the turbulence structure is postponed as the generation of large eddies around the inflection point of the profiles, probably caused by Kelvin-Helmholtz instabilities (see RAUPACH et al., 1996, for the *mixing layer analogy*), should be postponed until the larger vertical velocity gradients occur there.

A measure of flow equilibration over and within a canopy is the skewness of the velocity. The point of the adjustment is marked then by an *enhanced gust zone* with skewness values up to $Sk_u = 1.2$. It is predicted at a distance between 3h and 7h downwind from the windward forest edge at a height $z = 0.8h$ (see RAUPACH et al., 1987; DUPONT and BRUNET, 2008). Fig. 21 shows that we observe comparable Sk_u values already at T3 in a distance of 2h from the forest edge. Merely, the Sk_w is increasing between T3 and T4. The sign of Sk_u and Sk_w indicates that the turbulence within the crown space it dominated by downward gust. However, the passage through the canopy seems to destroy the structures quickly, and within the trunk space values below the typical $Sk_u \approx +0.5$ (see RAUPACH et al., 1996; FINNIGAN, 2000) are measured.

In contrast to the FM the LES shows an increasing SK_u and an *enhanced gust zone* (figures are given in SCHLEGEL et al., 2014) with $Sk_u > 1.2$ in the east of T4. This may be caused by the idealization of the stand in vegetation model, i.e. a more uniform *PAD*. The work of DUPONT et al. (2011) showed that for a canopy with a clear trunk space no *enhanced gust zone* has to occur, whereas in difference to this, an LES (DUPONT and BRUNET, 2008) using uniform vertical *PAD* profiles predicts an *enhanced gust zone*. Compared to these studies our results form a new case with a different canopy structure, which is characterized by a small clearing with a well developed forest edge, followed by canopy with a clear trunk space. The turbulence structure seems to adjust very fast to the canopy after the clearing. We assume two reasons for this behavior:

i) The clearing is small and the boundary layer above the canopy is not much affected by it.

Coherent structures can bridge the clearing and are measured directly behind it. Thus, we observe a layer with enhanced gust activity, but cannot see a clear positioned *enhanced gust zone* as in RAUPACH et al. (1987); DUPONT and BRUNET (2008).

ii) The forest edge is too dense to allow a steadily advective momentum entry causing a *sub-canopy jet* as it was the case in DUPONT et al. (2011). In consequence the adjustment of the sub-canopy flow is faster.

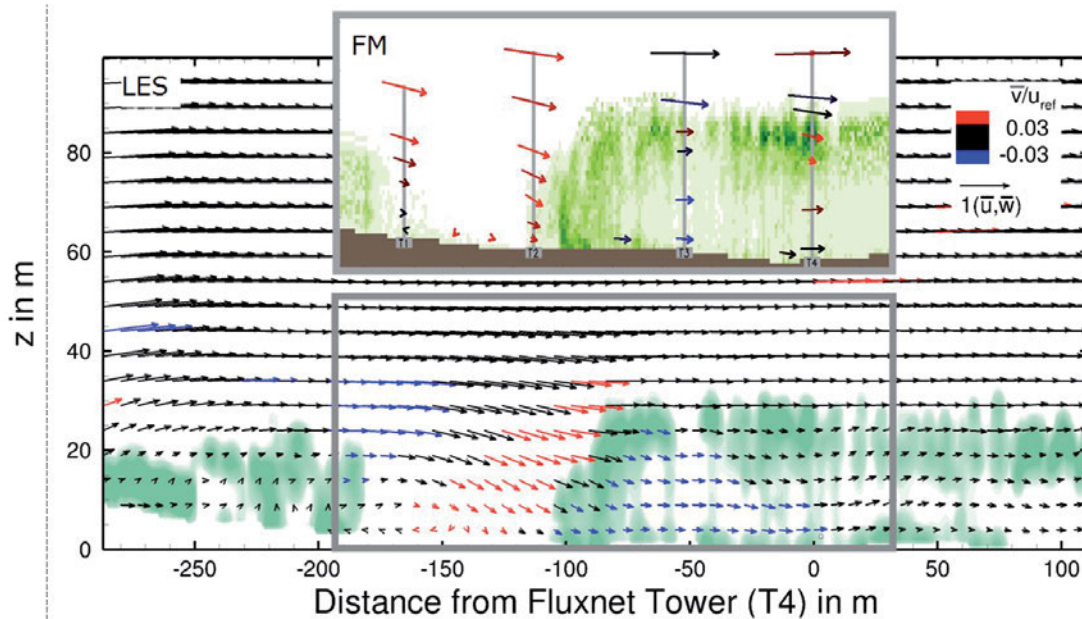


Figure 22: Mean velocity vectors (\bar{u} , \bar{v} , \bar{w}) in the plane $Y = 0$ from large-eddy simulation (LES case HET-Surf) and field measurements (FM). Coloring of the vector depicts the lateral velocity \bar{v} , with red colors indicating northward motion (into the picture) and blue southward motion (out of the picture). Background colors indicate the PAD. Within the larger graph, the lower outline of the vegetation marks the surface.

Over the forest clearing the SK_u and SK_w profiles of the FM and the LES show in accordance that the instability enhances the occurrence of gusts which transport momentum downwards to layers directly above the ground. There, they penetrate the forest edge which is revealed by the slightly increased SK_u at 2 m. However, the measured negative vertical velocity at T3 and T4, which feeds the sub-canopy flow is an indicator that the flow is still not in equilibrium at T4.

Above the canopy the wind measurements and also the model results indicate, that the influence of the clearing on the mean streamwise wind velocity vanishes fast with increasing distance (vertical as well as horizontal). At a height of 40 m almost no difference can be detected between T3 and T4.

6.4 Influences of topography

Another question is: How strong is the influence of the topography (i.e. the elevation) on the turbulent flow near the surface? Is the model domain large enough to represent all relevant components? In our case a small hill, the *S-Berg*, is located in the west of the site and several narrow valleys in the east and south (see Fig. 1). Despite the shallow terrain model of the LES (see Section 5.3), we observed an unexpected conformity of the LES and the FM results in Fig. 22. We may conclude, that the tilt angle of the average flow is rather determined by the local canopy structure than by the changes in terrain elevation further away. This is also indicated by the unsatisfactory results of the WT experiment which involves the most extensive terrain model but only a limited resolution of the canopy structure. Thus, for a simulation of

the energy and mass exchange between a forest and the atmosphere the refinement of the canopy model is more important than the consideration of the surrounding hills and valleys. However, this may be only valid for sites with high roughness and tall heterogeneous canopies.

The streamlines in Fig. 23, starting in each sub-figure at another tower, illustrate how the forest clearing dominates the flow. The air of the lower layers around T1 and T2 (Fig. 23a and b) has an origin far more south than the transect, and air parcels crossing T1 could leave the clearing in northward direction. The air crossing the lower layers of T2 is again moving southwards within the trunk space, which was already indicated by Fig. 22. This motion persists until T3. Whereas T3 and T4 do not ‘see’ the clearing at all as the air crossing these towers comes always from above the canopy. The complex patterns clearly illustrate that numerical simulations based on real vegetation models are indispensable for a consideration of advective components in energy and mass budgets of heterogeneous forests.

7 Summary and concluding remarks

Recent studies (e.g., CASSIANI et al., 2008; DUPONT et al., 2012) including this work demonstrated that the wind speed distribution in forests is dominated by inhomogeneities like step changes in stand height and forest clearings. Thus, a major limitation in the attempts to describe and model the wind field in tall canopies is the parametrization of the plant architecture.

Investigating a mixed conifer forest in a low mountain range, we used terrestrial laser scanning (TLS) to derive a three-dimensional vegetation model usable for

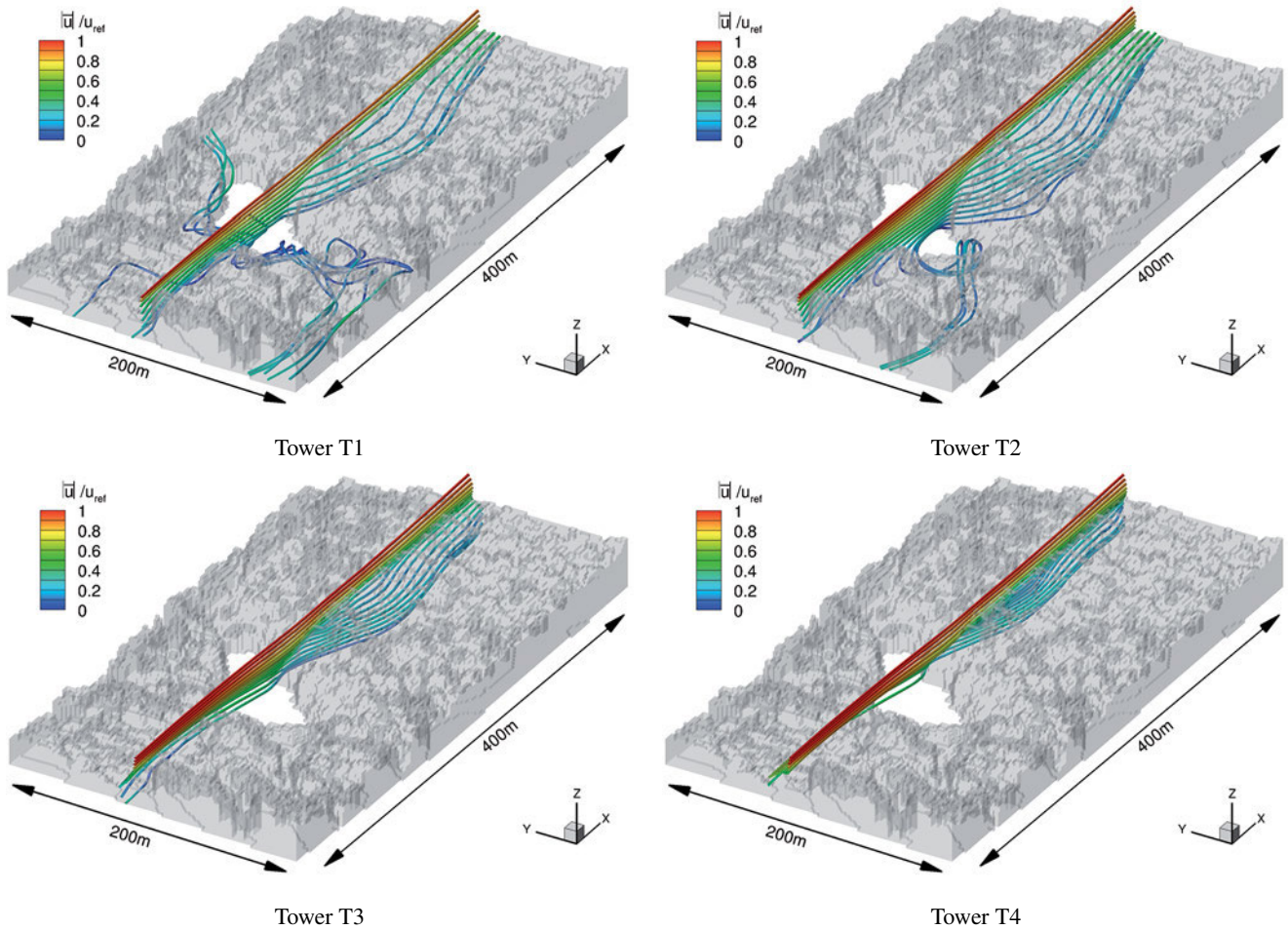


Figure 23: Streamlines of the mean flow passing the four measurement towers for HET-Surf. The streamlines are colored by the magnitude of the mean velocity. The gray shaded area represents the vegetation in terms of a plant area density greater than zero. The lower outline of the vegetation marks the surface. Please note that only a part of the computational domain is shown.

numerical models. Depending on the number of view points of the laser scanner and the plant area density, three-dimensional vegetation models with a minimal grid size of 0.5 m can be derived applying this new method.

The turbulent wind field across a forest clearing was observed over 17 520 hours by multi-level high-frequency wind velocity measurements applying 27 ultrasonic anemometers. These measurements enabled us to investigate the relationship between wind speed, drag coefficient and plant area distribution experimentally. We found a streamlining of the vegetation only in a thin layer at the canopy top. Contrary to a sheltering effect we observed an increasing drag coefficient with *PAD*, which is partly explained by different aerodynamic properties of conifer twigs with needles and smoother trunks. Based on these results, we do recommend to parameterize the drag coefficient as a function of the *PAD* in numerical models.

The TLS based vegetation parametrization was tested in two numerical model frames, a boundary layer model, which uses averaged Navier-Stokes equations and in large-eddy simulations, which resolve the dominant tur-

bulence structures. Both approaches showed significantly improved results evaluated by the field measurements. The BLM suffered mostly from the limits of the two dimensional model setup, which permits to depict mean turbulent flow adequately well, but is not sufficient to simulate the complex three-dimensional flow structure.

A wind tunnel experiment was conducted using a physical model of the site, which was build upon detailed topological information, but limited resolution of the stand structure. The simplified model of the canopy showed surprisingly good agreement with the field measurements within the stand and crown region. However, it was not capable to reproduce the turbulent flow over the clearing. Compared to numerical models, the project showed that the physical modeling in a wind tunnel is approaching its limits, due to insufficiently detailed representation of the vegetation structure.

The field measurements and the LES gave new insight into the structure of the turbulent flow over a clearing. The arising picture shows that the zones of intensive turbulence development cannot be restricted to the

locations found in previous studies with more idealized canopies.

Assessing the effect of small inhomogeneities like forest clearings or forest tracks on the turbulent flow in and above a tall canopy, attention must be paid to a significant deviation of the mean flow within the canopy whereas the influence is diminishing fast with height above the canopy.

Considering the exchange of scalars between atmosphere and surface, the resulting advective flows within the canopy are relevant and amplify the effect of the intermittent nature of the turbulence on the spatial inhomogeneity of the exchange. The parametrization of this effect in large scale atmospheric models is still not solved.

However, the occurrence of the advective flows is connected to surface conditions including the structure of the vegetation cover. Our work shows a way to implement vegetation models close to reality in numerical simulations, which is an important step to regard these inhomogeneities of the surface-atmosphere exchange in future.

Acknowledgments

The work was supported by the German National Science Foundation (Deutsche Forschungsgemeinschaft, DFG, funding codes: BE 1721/11-3, GO 1111/1-2, HI 1092/1-2, MA 2504/11-3, STI 157/3-3). The project “Turbulent Exchange processes between Forested areas and the Atmosphere” was a part of the DFG priority programme 1276 MetStröm: Multiple Scales in Fluid Mechanics and Meteorology. Computational facilities were provided by the Centre for Information Services and High Performance Computing (ZIH) of the Technische Universität Dresden. We gratefully acknowledge GIL BOHRER (Ohio State University), CHRISTIAN FEIGENWINTER and Dr. ROLAND VOGT (University of Basel) for their valuable comments and scientific discussions.

References

- ARMITT, J., J. COUNIHAN, 1968: The simulation of the atmospheric boundary layer in a wind tunnel. – *Atmos. Environ.* **2**, 49–62.
- ARYA, S.P., 2001: Introduction to micrometeorology. – Academic Press.
- AUBINET, M., 2008: Eddy covariance CO₂ flux measurements in nocturnal conditions: an analysis of the problem. – *Ecological Applications: A Publication of the Ecological Society of America* **18**, 1368–1378, PMID: 18767616.
- AUBINET, M., B. HEINESCH, C. BERNHOFER, E. CANEPA, A. LINDROTH, L. MONTAGNANI, C. REBMANN, P. SEDLAK, E. VAN GORSEL, 2010: Direct advection measurements do not help to solve the night-time CO₂ closure problem: Evidence from three different forests. – *Agricult. Forest Meteorol.* **150**, 655–664.
- AUBINET, M., T. VESALA, D. PAPALE (Eds.), 2012: Eddy Covariance: A Practical Guide to Measurement and Data Analysis. – Springer.
- AUBRUN, S., R. KOPPMANN, B. LEITL, M. MÖLLMANN-COERS, A. SCHAUB, 2005: Physical modelling of a complex forest area in a wind tunnel – comparison with field data. – *Agricult. Forest Meteorol.* **129**, 121–135.
- BALDOCCHI, D., E. FALGE, L. GU, R. OLSON, D. HOLLINGER, S. RUNNING, P. ANTHONI, C. BERNHOFER, K. DAVIS, R. EVANS, J. FUENTES, A. GOLDSTEIN, G. KATUL, B. LAW, X. LEE, Y. MALHI, T. MEYERS, W. MUNGER, W. OECHEL, K.T. PAW, K. PILEGAARD, H.P. SCHMID, R. VALENTINI, S. VERMA, T. VESALA, K. WILSON, S. WOFSY, 2001: FLUXNET: a new tool to study the temporal and spatial variability of Ecosystem-Scale carbon dioxide, water vapor, and energy flux densities. – *Bull. Amer. Meteor. Soc.* **82**, 2415–2434.
- BELCHER, S.E., N. JERRAM, J.C.R. HUNT, 2003: Adjustment of a turbulent boundary layer to a canopy of roughness elements. – *J. Fluid Mech.* **488**, 369–398.
- BIENERT, A., H.-G. MAAS, 2009: Methods for the automatic geometric registration of terrestrial laserscanner point clouds in forest stands. – *International Archives of Photogrammetry, Remote Sensing and Spatial Information Sciences* **38-3/W8**, 1–6.
- BIENERT, A., R. QUECK, A. SCHMIDT, C. BERNHOFER, H.-G. MAAS, 2010: Voxel space analysis of terrestrial laser scans in forests for wind field modelling. – *International Archives of Photogrammetry, Remote Sensing and Spatial Information Sciences* **38**, Part 5, 92–97.
- BIENERT, A., K. PECH, H.-G. MAAS, 2011: Verfahren zur Registrierung von Laserscannerdaten in Waldbeständen Schweizerische Zeitschrift für Forstwesen – methods for registration laser scanner point clouds in forest stands. – *Schweizerische Z. Forstwesen* **162**, 178–185.
- BOHRER, G., M. WOLOSIN, R. BRADY, R. AVISSAR, 2007: A virtual canopy generator (V-CaGe) for modelling complex heterogeneous forest canopies at high resolution. – *Tellus B* **59**, 566–76.
- BRUNET, Y., J.J. FINNIGAN, M.R. RAUPACH, 1994: A wind tunnel study of air flow in waving wheat: Single-point velocity statistics. – *Bound.-Layer Meteorol.* **70**, 95–132.
- CASSIANI, M., G.G. KATUL, J.D. ALBERTSON, 2008: The effects of canopy leaf area index on airflow across forest edges: Large-eddy simulation and analytical results. – *Bound.-Layer Meteorol.* **126**, 433–460.
- CESCATTI, A., B. MARCOLLA, 2004: Drag coefficient and turbulence intensity in conifer canopies. – *Agricult. Forest Meteorol.* **121**, 197–206.
- CLEMENT, R., 2004: Mass and energy exchange of a plantation forest in Scotland using micrometeorological methods. – Ph.D. thesis, University of Edinburgh.
- DEARDORFF, J., 1980: Stratocumulus-capped mixed layers derived from a three-dimensional model. – *Bound.-Layer Meteorol.* **18**, 495–527.
- DETTO, M., G.G. KATUL, M. SIQUEIRA, J. JUANG, P. STOY, 2008: The structure of turbulence near a tall forest edge: the backward-facing step flow analogy revisited. – *Ecological Appl.* **18**, 1420–1435.
- DUPONT, S., Y. BRUNET, 2008: Edge flow and canopy structure: A Large-Eddy simulation study. – *Bound.-Layer Meteorol.* **126**, 51–71.
- DUPONT, S., Y. BRUNET, 2009: Coherent structures in canopy edge flow: A large-eddy simulation study. – *J. Fluid Mech.* **630**, 93–128.
- DUPONT, S., J.-M. BONNEFOND, M.R. IRVINE, E. LAMAUD, Y. BRUNET, 2011: Long-distance edge effects in a pine forest with a deep and sparse trunk space: In situ and numerical experiments. – *Agricult. Forest Meteorol.* **151**, 328–344.

- DUPONT, S., M.R. IRVINE, J. BONNEFOND, E. LAMAUD, Y. BRUNET, 2012: Turbulent structures in a pine forest with a deep and sparse trunk space: Stand and edge regions. – *Bound.-Layer Meteor.* **143**, 309–336.
- FARO, 2005: Aufbruch in neue Dimensionen: Der FARO Laser Scanner LS. – Data Sheet Faro LSHE880.
- FEIGENWINTER, C., C. BERNHOFER, R. VOGT, 2004: The influence of advection on the short term CO₂-budget in and above a forest canopy. – *Bound.-Layer Meteor.* **113**, 201–224.
- FEIGENWINTER, C., C. BERNHOFER, U. EICHELHANN, B. HEINESCH, M. HERTEL, D. JANOUS, O. KOLLE, F. LAGERGREN, A. LINDROTH, S. MINERBI, U. MODEROW, M. MÖLDER, L. MONTAGNANI, R. QUECK, C. REBMANN, P. VESTIN, M. YERNAUX, M. ZERI, W. ZIEGLER, M. AUBINET, 2008: Comparison of horizontal and vertical advective CO₂ fluxes at three forest sites. – *Agricult. Forest Meteor.* **148**, 12–24.
- FINNIGAN, J.J., 2000: Turbulence in plant canopies. – *Ann. Rev. Fluid Mech.* **32**, 519–571.
- FISCHLER, M.A., R.C. BOLLES, 1981: Random sample consensus: a paradigm for model fitting with applications to image analysis and automated cartography. – *Commun. ACM* **24**, 381–395.
- FOKEN, T., B. WICHURA, 1996: Tools for quality assessment of surface-based flux measurements. – *Agricult. Forest Meteor.* **78**, 83–105.
- FRANK, C., B. RUCK, 2008: Numerical study of the airflow over forest clearings. – *Forestry* **81**, 259–277.
- FRÜHAUF, C., L. ZIMMERMANN, C. BERNHOFER, 1999: Comparison of forest evapotranspiration from ECEB-measurements over a spruce stand with the water budget of a catchment. – *Phys. Chem. Earth, Part B: Hydrol. Oceans Atmos.* **24**, 805–808.
- GRÜNWARD, T., C. BERNHOFER, 2007: A decade of carbon, water and energy flux measurements of an old spruce forest at the Anchor Station Tharandt. – *Tellus B* **59**, 387–396.
- GROSS, G., 1993: Numerical Simulation of Canopy Flows. – Springer Series in Physical Environment **12**.
- HEINEMANN, G., M. KERSCHGENS, 2006: Simulation of surface energy fluxes using high-resolution non-hydrostatic simulations and comparisons with measurements for the LITFASS-2003 experiment. – *Bound.-Layer Meteor.* **121**, 195–220.
- HIRAOKA, H., M. OHASHI, 2008: A (k- ϵ) turbulence closure model for plant canopy flows. – *J. Wind Engin. Indust. Aerodyn.* **96**, 2139–2149.
- JASAK, H., 1996: Error analysis and estimation for the finite volume method with applications to fluid flows. – Ph.D. thesis, Imperial College of Science, London.
- JONES, W., B. LAUNDER, 1972: The prediction of laminarization with a two-equation model of turbulence. – *Int. J. Heat Mass Trans.* **15**, 301–314.
- KRAUS, H., 2008: Grundlagen der Grenzschicht-Meteorologie. – Springer.
- LEE, X., 2000: Air motion within and above forest vegetation in non-ideal conditions. – *Forest Ecol. Management* **135**, 3–18.
- LILLY, D., 1967: The representation of small-scale turbulence in numerical simulation experiments. – In: Proceedings of the IBM Scientific Computing Symposium on Environmental Sciences, number 320-1951 in IBM Form, 1–24. International Business Machines Corporation.
- LUMLEY, L., H. PANOFKY, 1964: The Structure of Atmospheric Turbulence – Interscience Pub., 239 pp.
- MAAS, H.-G., A. BIENERT, S. SCHELLER, E. KEANE, 2008: Automatic forest inventory parameter determination from terrestrial laser scanner data. – *Int. J. Remote Sens.* **29**, 1579–1593.
- MAHRT, L., D. VICKERS, J. SUN, N.O. JENSEN, H. ALLEN, E. PARDYJAK, H. FERNANDO, 2001: Determination of the surface drag coefficient. – *Bound.-Layer Meteor.* **99**, 249–276.
- MODEROW, U., C. FEIGENWINTER, C. BERNHOFER, 2007: Estimating the components of the sensible heat budget of a tall forest canopy in complex terrain. – *Bound.-Layer Meteor.* **123**, 99–120.
- PETERS, K., R. EIDEN, 1992: Modelling the dry deposition velocity of aerosol particles to a spruce forest. – *Atmos. Environ.* **26A**, 2555–2564.
- PINARD, J.D.J.-P., J.D. WILSON, 2001: First- and second-order closure models for wind in a plant canopy. – *J. Appl. Meteor.* **40**, 1762–1768.
- QUECK, R., C. BERNHOFER, 2010: Constructing wind profiles in forests from limited measurements of wind and vegetation structure. – *Agricult. Forest Meteor.* **150**, 724–735.
- QUECK, R., A. BIENERT, H.-G. MAAS, S. HARMANSA, V. GOLDBERG, C. BERNHOFER, 2012: Wind fields in heterogeneous conifer canopies: parameterisation of momentum absorption using high-resolution 3D vegetation scans. – *European J. Forest Res.* **131**, 165–176.
- RAUPACH, M.R., A.S. THOM, 1981: Turbulence in and above plant canopies. – *Ann. Rev. Fluid Mech.* **13**, 97–129.
- RAUPACH, M., E.F. BRADLEY, H. GHADIRI, 1987: A wind tunnel investigation into aerodynamic effect of forest clearings on the nesting of abbot's booby on christmas island. – Tech. rep., CSIRO Centre for Environmental Mechanics, Canberra.
- RAUPACH, M.R., J.J. FINNIGAN, Y. BRUNET, 1996: Coherent eddies and turbulence in vegetation canopies: The mixing-layer analogy. – *Bound.-Layer Meteor.* **78**, 351–382.
- RIEGL, 2009: Long range & high accuracy 3D terrestrial laser scanner system. – LMS-Z420i. data sheet LMS-Z420i.
- ROSEMEIER, G., 2009: Windbelastung von Bauwerken: Hoch- und Brückenbauten, Schalen, leichte Flächentragwerke; neue Windlastnorm DIN 1055-4; Baudynamik, Aerodynamik, Luftturbulenzen. – Bauwerk, Berlin.
- SANTIAGO, J., A. DEJOAN, A. MARTILLI, F. MARTIN, A. PINELLI, 2010: Comparison between large-eddy simulation and reynolds-averaged Navier-Stokes computations for the MUST field experiment. Part I: Study of the flow for an incident wind directed perpendicularly to the front array of containers. – *Bound.-Layer Meteor.* **135**, 109–132.
- SCHLEGEL, F., J. STILLER, A. BIENERT, H.-G. MAAS, R. QUECK, C. BERNHOFER, 2012: Large-eddy simulation of inhomogeneous canopy flows using high resolution terrestrial laser scanning data. – *Bound.-Layer Meteor.* **142**, 223–243.
- SCHLEGEL, F., J. STILLER, A. BIENERT, H.-G. MAAS, R. QUECK, C. BERNHOFER, 2014: Large-eddy simulation study of a heterogeneous forest at sub-tree resolution. – *Bound.-Layer Meteor.* DOI:10.1007/s10546-014-9962-y.
- SCHMIDT, H., U. SCHUMANN, 1989: Coherent structure of the convective boundary layer derived from large-eddy simulations. – *J. Fluid Mech.* **200**, 511–562.
- SCHWÄRZEL, K., A. MENZER, F. CLAUSNITZER, U. SPANK, J. HÄNTZSCHEL, T. GRÜNWARD, B. KÖSTNER, C. BERNHOFER, K.-H. FEGER, 2009: Soil water content measurements deliver reliable estimates of water fluxes: A comparative study in a beech and a spruce stand in the Tharandt forest (Saxony, Germany). – *Agricult. Forest Meteor.* **149**, 1994–2006.
- SHAW, R., E. PATTON, 2003: Canopy element influences on resolved- and subgrid-scale energy within a large-eddy simulation. – *Agricult. Forest Meteor.* **115**, 5–17.
- SHAW, R.H., U. SCHUMANN, 1992: Large-eddy simulation of turbulent flow above and within a forest. – *Bound.-Layer Meteor.* **61**, 47–64.
- SHAW, R., G. DEN HARTOG, H. NEUMANN, 1988: Influence of foliar density and thermal stability on profiles of Reynolds stress and turbulence intensity in a deciduous forest. – *Bound.-Layer Meteor.* **45**, 391–409.

- SOGACHEV, A., O. PANFEROV, 2006: Modification of two-equation models to account for plant drag. – *Bound.-Layer Meteor.* **121**, 229–266.
- SOGACHEV, A., G.V. MENZHULIN, M. HEIMANN, J. LLOYD, 2002: A simple three-dimensional canopy - planetary boundary layer simulation model for scalar concentrations and fluxes. – *Tellus B - Chem. Phys. Meteor.* **54**, 784–819.
- SUN, H., 2005: Numerical simulation of canopy flow and carbon dioxide flux at the west coast flux station. – Master thesis, University of British Columbia.
- TAYLOR, G.I., 1938: The spectrum of turbulence. – *Proceedings of the Royal Society of London. Series A – Mathematical and Physical Sciences* **164**, 476–490.
- THOM, A.S., 1971: Momentum absorption by vegetation. – *Quart. J. Roy. Meteor. Soc.* **97**, 414–428.
- VOSSELMAN, G., H.-G. MAAS, 2010: Airborne and terrestrial laser scanning. – Whittles Publishing, Dunbeath.
- WELLER, G., G. TABOR, H. JASAK, C. FUREBY, 1998: A tensorial approach to computational continuum mechanics using object-oriented techniques. – *Comp. Phys.* **12**, 620–631.
- YANG, B., M.R. RAUPACH, R.H. SHAW, K.T. PAW U, A. MORSE, 2006: Large-eddy simulation of turbulent flow across a forest edge. Part I: Flow statistics. – *Bound.-Layer Meteor.* **120**, 377–412.
- ZENG, P., H. TAKAHASHI, 2000: A first-order closure model for the wind flow within and above vegetation canopies. – *Agricult. Forest Meteor.* **103**, 301–313.